

# Controlling factors analysis for the Himawari-8 aerosol optical depth accuracy from the standpoint of size distribution, solar zenith angles and scattering angles

Ming Zhang<sup>a</sup>, Yingying Ma<sup>b,\*</sup>, Yifan Shi<sup>c,1</sup>, Wei Gong<sup>b</sup>, Shihua Chen<sup>c</sup>, Shikuan Jin<sup>b</sup>, Jun Wang<sup>d</sup>

<sup>a</sup> Hubei Key Laboratory of Critical Zone Evolution, School of Geography and Information Engineering, China University of Geosciences, Wuhan, 430074, China

<sup>b</sup> State Key Laboratory of Information Engineering in Surveying, Mapping and Remote Sensing, Wuhan University, China

<sup>c</sup> School of Mathematics and Statistics, Wuhan University, China

<sup>d</sup> Department of Chemical and Biochemical Engineering, Center for Global & Regional Environmental Research, The University of Iowa, Iowa City, IA 52242, USA

## HIGHLIGHTS

- The lower default fine-mode median radius is one of the main reason which leads the underestimate of AHI AOD.
- Comparison with in situ data reveals that the phase function greatly affects the AOD retrieval.
- The dark target method was introduced for AHI retrieval, showing poor performance in high AOD condition.

## ARTICLE INFO

### Keywords:

Advanced himawari imager  
Aerosol optical depth  
Size distribution  
Solar zenith angles  
Scattering angles

## ABSTRACT

This work aims at providing a novel controlling factors analysis for the Advanced Himawari Imager (AHI) AOD retrieval from the aspect of particle size distribution and Sun-Earth-Satellite geometries, through combining the high quality ground-based observation in Wuhan. The three-years co-located AOD dataset of AHI and sun-photometer in Wuhan are used to support this work. AHI overall underestimates AOD over Wuhan site with coefficient of determination ( $R^2$ ) equal 0.7. Though the best retrieval appeared in summer, underestimation is found to be persistent in each season. Combining with the characteristics of aerosol hygroscopic growth in Wuhan, we found the fine-mode particle median radius which supposed by AHI is lower than the in-site measurement. This leads to the overestimation of back scattering by aerosol particles, and induces underestimation of AOD consequently. The correlation and bias analyses of AOD with respect to the variation of Solar Zenith Angle and scattering angles are also performed. Phase function derived by sun-photometer is applied to discuss the influence of scattering angle on AOD inversion. Accompany with the scattering angle, the AOD retrieval bias consistently varies with the phase function bias, which further confirm the impact of phase function on AHI retrieval. Finally, the dark target method was applied to retrieve AHI AOD. The comparison results show that dark target overestimated AOD and performed worse in Wuhan. It could reveals that AHI aerosol retrieval method has some advantages in heavy aerosol loading places without enough prior information of aerosol properties.

## 1. Introduction

Natural processes and human activities produce a large amount of aerosols, of which high concentrations are commonly found in urban and desert areas (Liou, 2002). The sizes of aerosol particles usually range

from approximately  $10^{-3}$   $\mu\text{m}$ –100  $\mu\text{m}$ . Aerosols have been widely proven to greatly affect human health (Hinds, 1999; WHO, 2000), radiation (Atwater, 1970; Charlson et al., 1992; Mitchell, 1971) and climate (McCormick and Ludwig, 1967). Although previous studies have acknowledged the importance of aerosols in atmospheric research, some

\* Corresponding author.

E-mail address: [yym863@whu.edu.cn](mailto:yym863@whu.edu.cn) (Y. Ma).

<sup>1</sup> These authors contributed equally to this work.

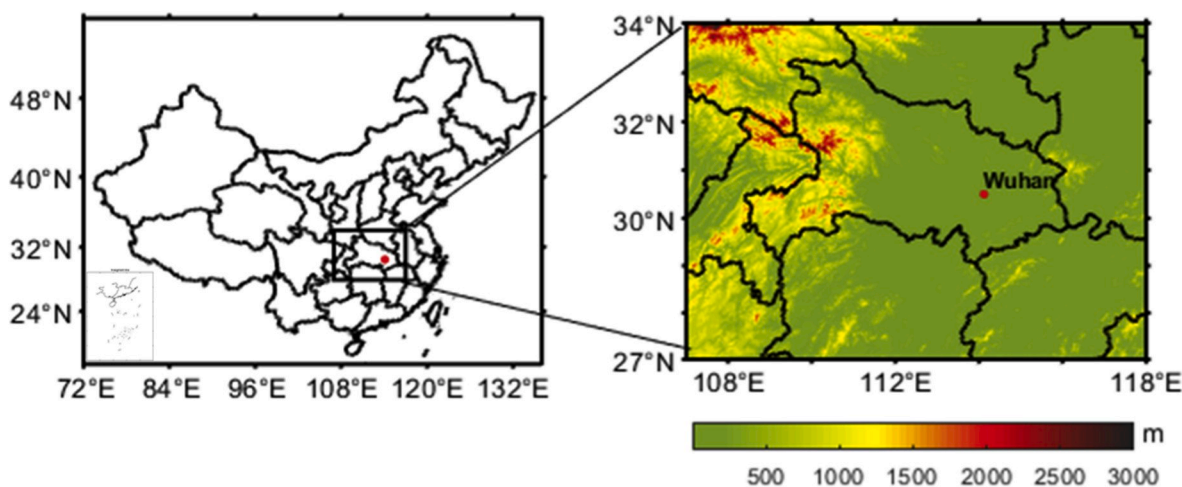


Fig. 1. Site location of the Wuhan University ground-based observation station.

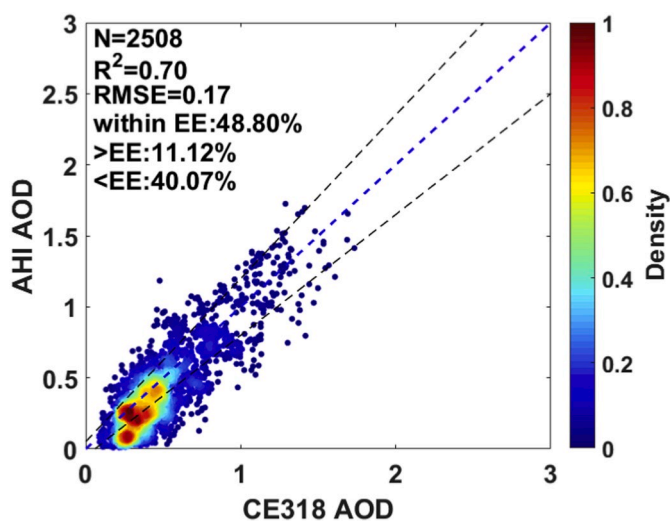


Fig. 2. Comparison of AHI AOD and CE-318 AOD. The blue dashed line denotes the 1:1 line, and the black dashed lines represent the line of EE. 11% of the samples are above the EE, whereas 40% are below the EE. The color represents how dense the samples are, and is determined by using the voronoi cell (Karimipour and Ghandehari, 2013). (For interpretation of the references to color in this figure legend, the reader is referred to the Web version of this article.)

uncertainties remain in our limited understanding of the distribution and physical and chemical properties of aerosols as well as the aerosol–cloud interaction (Winker et al., 2010; Yu et al., 2006).

As a fundamental optical property of aerosols, aerosol optical depth (AOD,  $\tau$ ) can characterize the degree of atmospheric turbidity and plays necessary roles in quantifying aerosol observation (Holben et al., 2001), estimating surface aerosol concentration (Wang and Christopher, 2003), calculating energy budget (Bellouin et al., 2005; Carslaw et al., 2013), and estimating the aerosol influence on cloud formation (Li et al., 2018) and boundary layer processes (Ge et al., 2014). The widely used passive remote sensing measurements to obtain AOD can be divided into two categories which are ground-based sun photometric and satellite-based observations. In view of the robust error analysis and outstanding quality control of sun photometric data (Dubovik et al., 2000), direct-sun measurements or photometers are often considered as the most reliable source of AOD data and have been widely used in validating AOD that are retrieved by various satellite sensors. These sensors have wide range of space observation applications and have become important sources of data for regional aerosol research (Kahnet et al.,

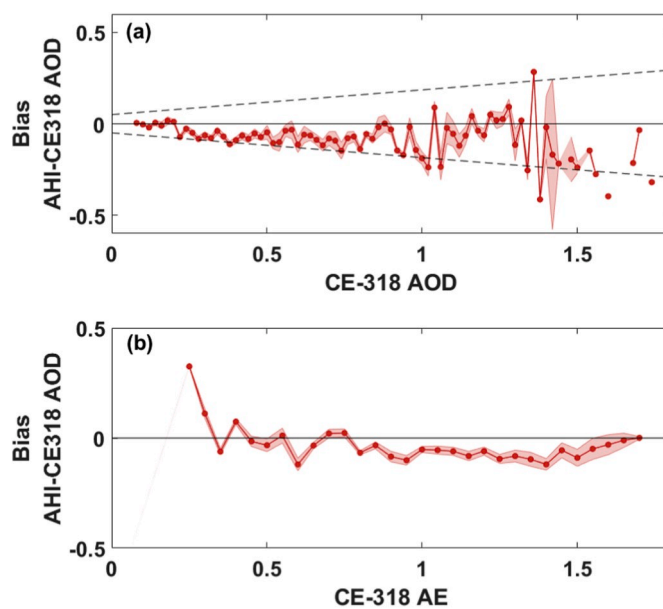
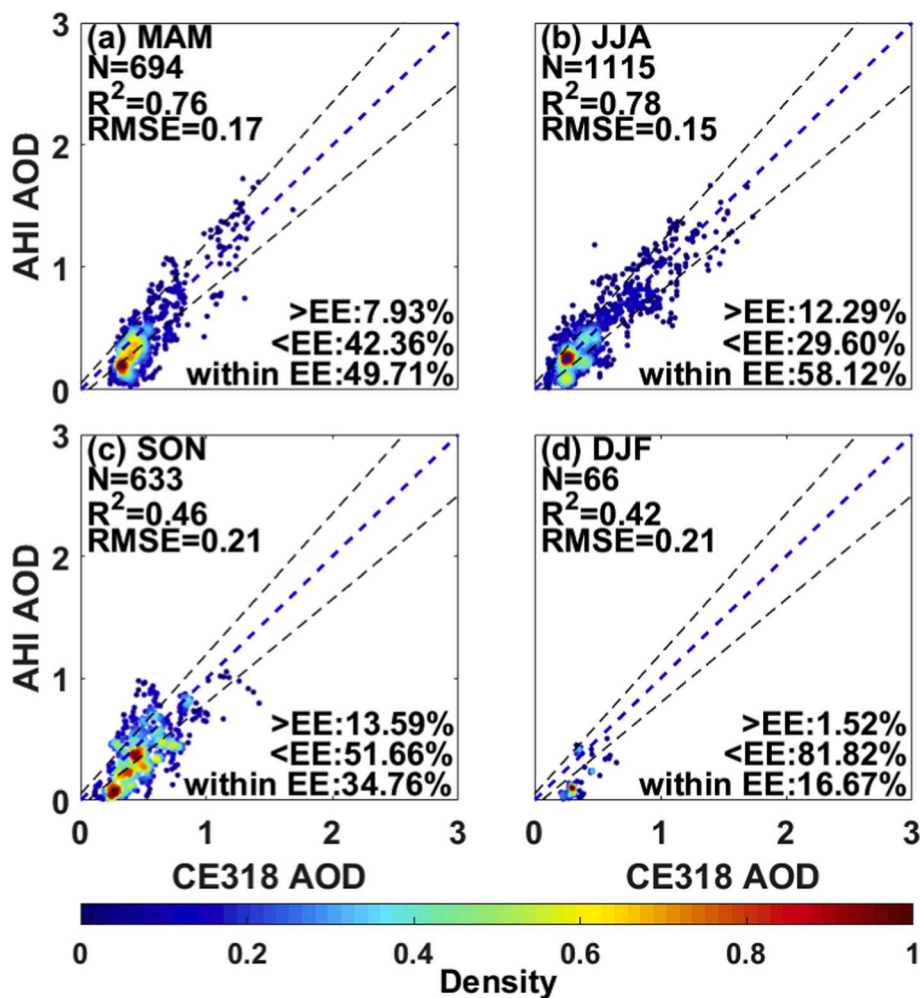


Fig. 3. The variation of AHI AOD bias (red circle) and variance (red shadow) with AOD (y-axis) for AOD (a) and 440 nm–675 nm CE-318 AE (b) varies. The black dashed lines express the EE. (For interpretation of the references to color in this figure legend, the reader is referred to the Web version of this article.)

2005; Remer et al., 2005; Winker et al., 2009). For example, the AOD provided by Moderate Resolution Imaging Spectroradiometer (MODIS) is one of the most successful examples of satellite-retrieved AOD with an uncertainty within  $\pm 0.05 \pm 0.15\tau$  (Levy et al., 2007b). However, in consideration of that MODIS is carried by the polar satellite and its data has low temporal resolution, MODIS has limitation on describing the diurnal change of AOD, aerosol radiative forcing, and surface  $PM_{2.5}$  which can be characterized by geostationary satellite (Wang et al., 2003a, 2003b, 2003c; Christopher et al., 2003; Lennartson et al., 2018). Advanced Himawari Imager (AHI) carried by a geostationary meteorological satellite named Himawari-8 has great advantages in temporal resolution as 10 min for its level-2 aerosol optical property product, thus makes it possible to observe the diurnal variation of AOD.

However, validation and analysis for the accuracy through controlling factors must be performed before applying AHI AOD. Yoshida et al. (2018) develop the AHI retrieval algorithm and perform a validation by using data from MODIS and 19 Aerosol Robotic Network (AERONET) sites. The retrieval shows a good correlation coefficient of 0.59 with



**Fig. 4.** Correlation analysis between AHI and CE-318 AOD across different seasons: (a) spring, (b) summer, (c) autumn, and (d) winter. The blue dashed line represents the 1:1 line, and the black dashed line represent the line of EE. (For interpretation of the references to color in this figure legend, the reader is referred to the Web version of this article.)

AERONET, and the researchers contribute error to the simulation of aerosol properties. Wang et al. (2019) performed a validation of AHI aerosol retrieval in full scene and recorded determinations coefficient ( $R^2$ ) of 0.61 with AERONET sites. This work attributed uncertainties to aerosol model, cloud filters and ground reflectance. Zhang et al. (2019) performed a validation using data from 16 AERONET sites and Sun-sky Radiometer Observation Network (SONET) sites all over China. This work also attributed the uncertainties of AHI retrieval to the simulation of aerosol models. Although previous studies have indicated the influence of aerosol model simulation, comparison between simulated and observed aerosol properties such as aerosol size distribution (ASD) and phase function are also need to be analyzed to better estimate their influences on AHI retrieval (Wang et al., 2003c).

This study performs our work by using the three-year (2016–2018) level-2 AOD dataset of AHI with observations from a well-maintained co-located sun photometer and evaluating the performance of AHI AOD retrieval in Wuhan, Central China. With its rapid economic development, Wuhan has suffered terrible aerosol pollution events over recent years; the aerosol pollution levels in this area may be worse than that recorded in traditional polluted places (Liu et al., 2018a,b; Zhang et al., 2018). Wuhan also has frequent cloudy conditions which hinder aerosol observation for satellite (Wang et al., 2017a); therefore, polar orbit satellites with low temporal resolution often fail to retrieve AOD in this area. Benefiting from its 10-min temporal resolution, AHI could provide enough observation here and support the detailed analyses

performed in this study. Except for seasonal and diurnal comparison between AHI AOD and a sun photometer AOD in Wuhan, we also analyzed the influence of ASD and phase function on AHI aerosol retrieval. Angles like solar zenith angle (SZA) and scattering angle may also affect AHI AOD retrieval but lack detailed discussion in former study. Wang et al. (2003c) showed that the effect of aerosol phase function was distinct in the AOD retrievals from geostationary satellite because the sensor on geostationary platform could measure the back-scatter for a wide range of scattering angles on a given day for a given aerosol layer. They show that the phase functions for both spherical and non-spherical particles should be considered in the retrieval of dust AOD. Here, with new generation of geostationary satellites such as Himawari, we further analyze how the accuracy of AOD retrieval varies with SZA ( $\theta$ ) or scattering angle ( $\Theta$ ) and give explanations based on transmission path and phase function. As this study focuses more on discussing the influence of aerosol characteristics and angles on AHI AOD retrieval, high temporal resolution data from a single site may help to prevent some disturbance, for example, the difference of surface albedo and satellite zenith angle. Through these analyses, we would obtain some more detailed insights about error sources and their influences, and these works can provide basis toward refining the accuracy of AOD retrieval. Finally, we applied the dark target (DT) method to AHI data retrieval. By comparing the AOD retrieved by the DT method and AHI's operational AOD, we reveal the effect of different AOD retrieval methods and illustrate the robustness of our findings.

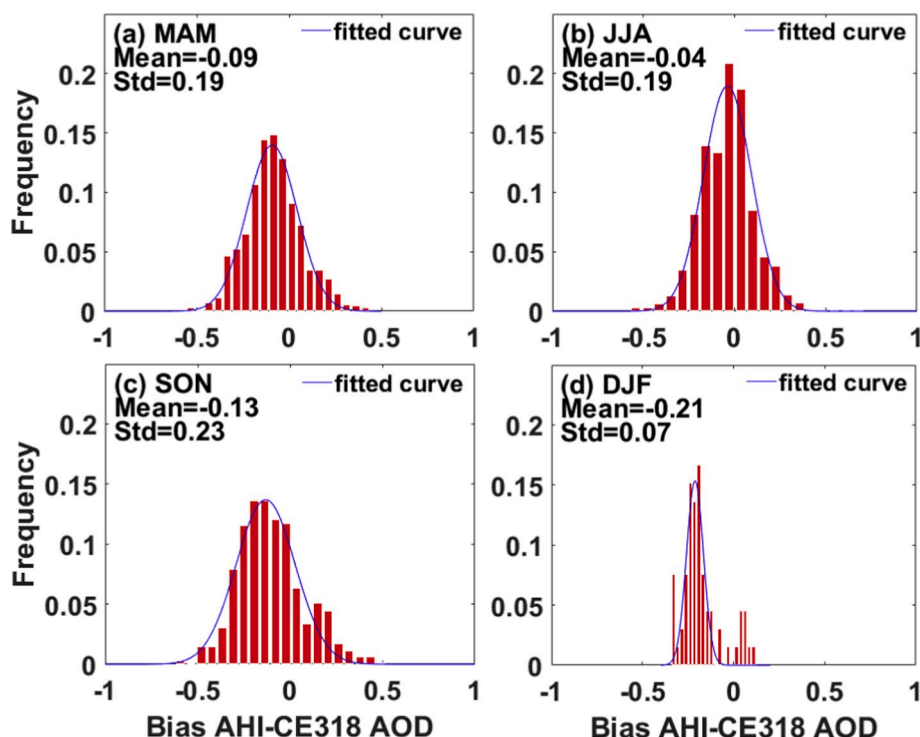


Fig. 5. Distribution of bias (AHI AOD minus CE-318 AOD, red bar) and the Gaussian distribution fitted curve (blue line). (For interpretation of the references to color in this figure legend, the reader is referred to the Web version of this article.)

This paper is organized as follows. Section 2 presents the data sources and the space-time matching method. Section 3 gives comparison between AHI AOD and CE-318 AOD under different aerosol properties, seasons, SZAs and scattering angles firstly. After that analysis on ASD and phase function are performed to give explanation. The DT method retrieved AHI AOD are also involved and provide comparison with AHI aerosol retrieval method at last. Section 4 concludes the paper.

## 2. Data and methods

### 2.1. AHI/Himawari-8 and MODIS

Himawari-8 is a new generation of Japanese geostationary meteorological satellites which carries a state-of-the-art optical sensor named AHI with significantly higher radiometric, spectral, and spatial resolutions compared with sensors that are previously available in the geostationary orbit (Bessho et al., 2016). The short revisit time (about 10 min for full disk) of AHI allows users to identify and track rapidly changing weather phenomena and derive quantitative products. The level-2 AHI aerosol optical property products with 10-min temporal resolution and 5-km spatial resolution retrieved from January 2016 to September 2018 are used in this study. The product contains AOD data at 500 nm, single-scattering albedo at 500 nm, and 400 nm–600 nm Ångström exponent (AE). The level-2 retrieval algorithm of AHI is based on the works of Higurashi and Nakajima (1999) and Fukuda et al. (2013), and it uses a radiative transfer code developed by Nakajima and Tanaka (1988) and Stamnes et al. (1988) and a look-up table to simulate radiation in different wavelengths and then applies an optimal estimate method adapted from Rodgers (2000) to retrieve AOD. Other components of this algorithm include the cloud detection algorithm adapted from Ishida and Nakajima (2009), Ishida et al. (2011), a fine aerosol model adapted from Omar et al. (2005). The retrieval process is presented in the work of Yoshida et al. (2018).

MODIS is a key instrument of the Earth Observing System launched onboard the Terra (which descends southward at 10:30 local time) and

Aqua (which ascends northward at 13:30 local time). The MODIS level-2 atmospheric aerosol product (MOD for Terra and MYD for Aqua) provides a global coverage of aerosol properties retrieved by the DT and deep blue (DB) algorithms. While the DT algorithm is applied over ocean and dark land, the DB algorithm covers the entire land (Kaufman and Tanré, 1998; Levy et al., 2007a, 2013). The MODIS aerosol product has been widely validated and used (Chu et al., 2002; Remer et al., 2002; Tao et al., 2015, 2017a; Wei et al., 2019). In this study, we use AOD from the “Corrected\_Optical\_Depth\_Land” dataset of MOD04 and MYD04 in version 6.1, which is derived by the DT method. AOD in 0.47, 0.55, and 0.66  $\mu\text{m}$  wavelengths from this dataset are transformed to AOD in 0.5  $\mu\text{m}$  wavelength to compare with AHI AOD.

### 2.2. Site and sun photometer

The Wuhan University ground-based atmospheric observation station is located at the top of the State Key Laboratory of Information Engineering in Surveying, Mapping, and Remote Sensing (114.37° E; 30.53° N) in Wuhan, Hubei Province, China, as shown in Fig. 1. This station has more than 10 types of instruments for ground-based observation, including a Cimel sun photometer (CE-318, installed in July 2007), a microwave radiometer, a multi-filter rotating shadow band radiometer, and a Mie-Raman Lidar. The CE-318 is calibrated every year using CARsNET (China Meteorological Administration Aerosol Remote Sensing Network) reference instrument under stable atmosphere and low aerosol loading.

CE-318 conducts direct spectral solar radiation measurements within a 1.2° full field of view every 15 min (Holben et al., 1998). Measurements from 8 channels (340, 380, 440, 500, 670, 870, 1020, and 1640 nm) are used to obtain the spectral AOD (Dubovik et al., 2000; Holben et al., 1998), and the total uncertainty in AOD is approximately 0.01–0.02 (Eck et al., 1999). The bundled software of CE-318, called ASTP, provides AOD in 8 channels and the AE. Observations from January 2016 to September 2018 are used to match the AOD retrieval data of AHI and to make validation.

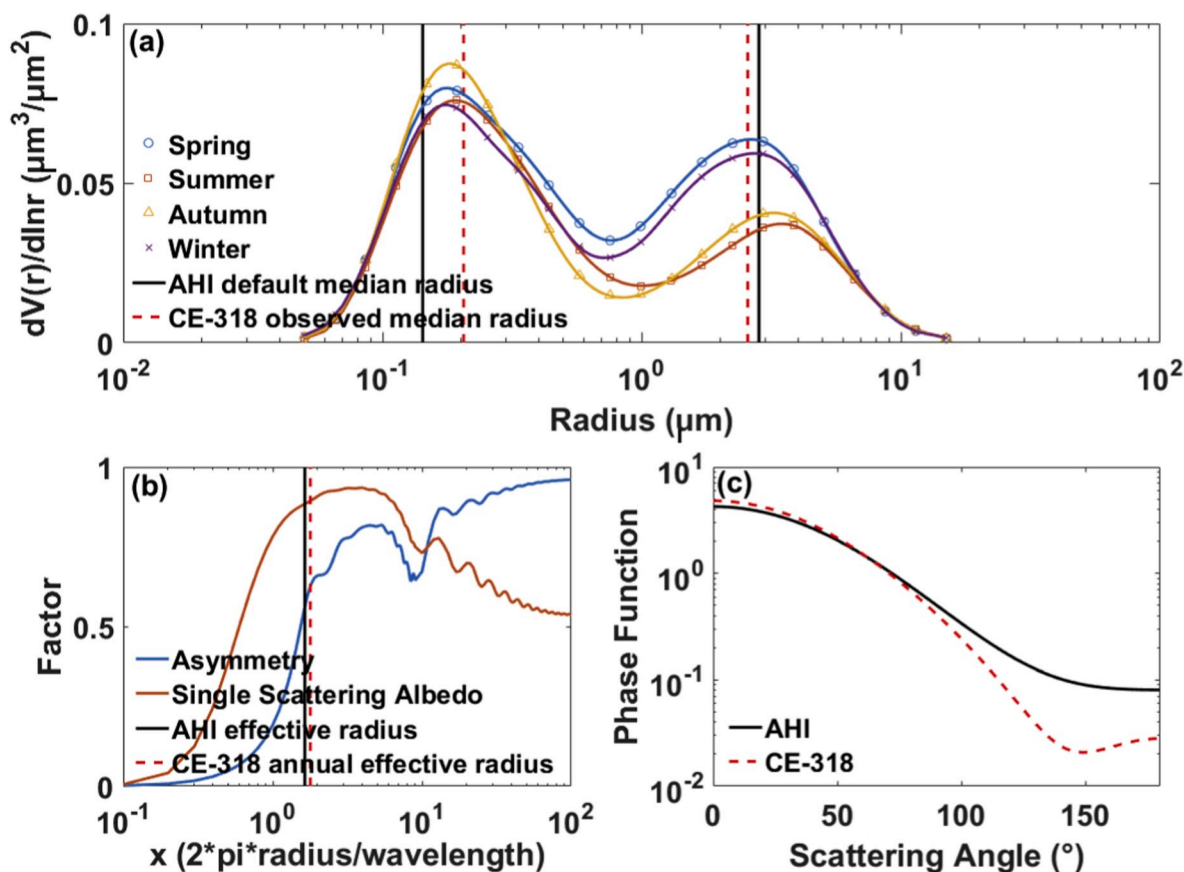


Fig. 6. (a) Seasonal average aerosol size distribution in spring (blue), summer (red), autumn (yellow), and winter (purple) in Wuhan as observed by CE-318. (b) Variation of asymmetry factor (blue) and the ratio of back-scattering and extinction efficiency (red) of fine-mode particle along with size parameter ( $x$ ) for the spherical Mie scattering algorithm. (c) Phase function simulated by using AHI effective radius (black line) and CE-318 annual effective radius (red dashed line). (For interpretation of the references to color in this figure legend, the reader is referred to the Web version of this article.)

### 2.3. Evaluation method

The coefficient of determination ( $R^2$ ), root mean square deviation (RMSE), bias (AHI AOD – CE-318 AOD), and percentage of AHI AOD falling within the expected error (EE) range ( $\pm 0.05 \pm 0.15\tau$ ) are used to evaluate AHI AOD retrieval. The  $R^2$  is interpreted as the proportion of the variance in the dependent variable that is predictable from the independent variable, and is an indicator indicating the reliability of changes in dependent variables. RMSE is the square root result of linear regression loss function, and it reveals the absolute difference between two variables. Bias refers to the tendency of a measurement process to over- or under-estimate the value of a population parameter, and AOD from CE-318 is used as compare object in this work. The EE range refers to (Remer et al., 2005). The temporal-spatial matching method is adapted from previous studies (Liu et al., 2014a,b; Nichol and Bilal, 2016; Wang et al., 2017a,b; Xiao et al., 2016). AHI retrieval AOD in Wuhan is computed by averaging all retrieved AOD with quality flag of good in an  $8 \times 8$  gridding focusing on Wuhan University site. In order to obtain a representative AHI AOD, 20% of the grid points in the  $8 \times 8$  gridding should have effective AOD, or the averaged value at this time would be abandoned. We adopt the 20% standard from Huang et al. (2016). For temporal match, AOD from CE-318 should have 2 or more observations within 30 min centered on the AHI measuring time, or this match fails.

### 2.4. SZA, scattering angle and their roles in radiative transfer model

The basic radiative transfer equation for diffused solar radiation under an assumed plane-parallel scattering atmosphere is formulated as

follows (Liou, 2002):

$$-\cos \theta \frac{dI(\tau, \Omega)}{d\tau} = -I(\tau, \Omega) + \frac{\varpi}{4\pi} F_0 e^{-\frac{\tau}{\cos \theta_0}} P(\Omega, \Omega_0) + \frac{\varpi}{4\pi} \int_{4\pi} I(\tau, \Omega') P(\Omega, \Omega') d\Omega' + B[T(\tau)] \quad (2.4.1)$$

where  $I(\tau, \Omega)$  is the specific intensity at optical depth  $\tau$  along unit vector  $\Omega$ ,  $\Omega$  lies in the direction  $(\theta, \phi)$  that represents the satellite zenith and azimuth angles, respectively, while  $\Omega_0$  lies in the direction  $(\theta_0, \phi_0)$  that represents the solar zenith and azimuth angles.  $\varpi$  and  $P$  represent the single scattering angle and phase function of air mass.  $F_0$  represents the flux density of solar radiation.  $B [T(\tau)]$  is the Planck function and it represents emission.

SZA ( $\theta_0$ ) refers to the angle between the zenith and the sun disc center (Hartmann, 2015) and complements the solar elevation angle. The SZA determines the transfer path and affects scattering. The radiative transfer path increases along with an increasing SZA. Under an assumed plane-parallel scattering atmosphere, a longer path may introduce additional errors in the calculation of the extinction part (the first term on the right-hand side of formula (2.4.1)). Moreover, the multiple scattering calculation in radiative transfer models are all simplified, so a longer path which causes more multiple scattering may also introduce additional errors in the scattering simulation.

Meanwhile, relative azimuth angle represents the relative azimuth of the sun's position and satellite position and is calculated by the sun azimuth angle ( $\phi_0$ ) and the satellite azimuth angle ( $\phi$ ). Given that Himawari-8 is a geostationary satellite, the satellite solar angle and satellite azimuth angle of Wuhan station are both fixed.

Scattering angle ( $\Theta$ ) refers to the angle between the extension lines of

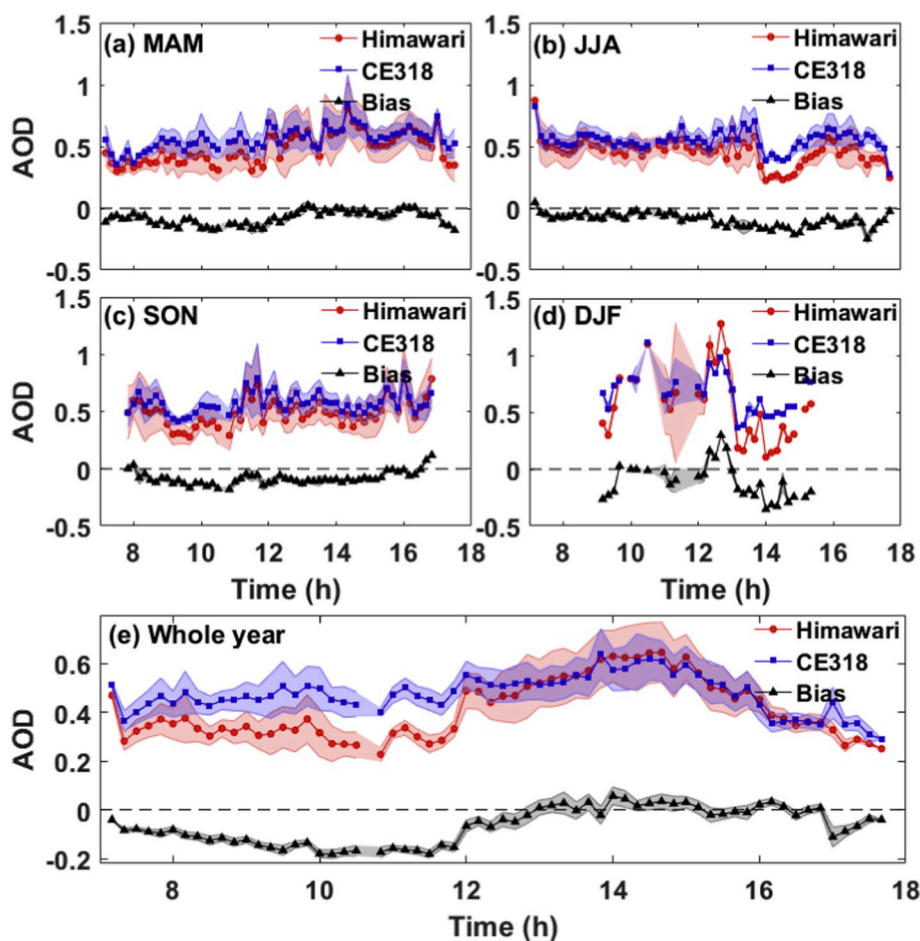


Fig. 7. Seasonal and annual average of diurnal variations of AHI (red circle and line) and CE-318 (blue cube and line) AOD as well as their bias (black triangle and line) during 2016–2018. (For interpretation of the references to color in this figure legend, the reader is referred to the Web version of this article.)

the incident and outgoing directions (Levy, 2009). This angle can be calculated using formula (2.4.2). The scattering angle participates in formula (2.4.1) through the scattering phase function ( $P$ ) where the scattering angle is presented by  $(\Omega, \Omega_0)$ .

$$\cos\Theta = -\cos\theta\cos\theta_0 + \sin\theta\sin\theta_0\cos(\phi - \phi_0) \quad (2.4.2)$$

### 2.5. The dark target method for AHI AOD retrieval

The dark target (DT) method is designed to infer clear-sky aerosol properties from MODIS observation over land surfaces that have low values of surface reflectance in parts of the visible and shortwave infrared spectrum (Levy et al., 2010). The basic algorithm is developed by Kaufman et al. (1997) and improved by many other researchers (Ackerman et al., 1998; Martins et al., 2002; Levy et al., 2007b; Li et al., 2005). The Dark Target method used here is based on the basic DT algorithm and the improvements. The aerosol models we used are the moderately absorbing aerosol model and coarse-dominated model (dust) (Levy et al., 2007a; Remer and Kaufman, 1998), and the cloud mask method we used is the method for MODIS C006-L (Levy et al., 2013). This cloud masking method is proposed by Martins et al. (2002) with a  $3 \times 3$  standard deviation sliding window. The corresponding threshold values for cloud masking and surface reflectance estimating refer to the work of Ge et al. (2019). They use a new NDVI of AHI sensor to improve the surface reflectance estimation based on DT method after analyzing the spectral characteristics of the sensor. The spatial and temporal matches for the dark target method are consistent with those for the evaluation method discussed in section 2.3.

## 3. Results and discussion

This section performs correlation and bias analysis of AHI and CE-318 AOD under different AOD, Ångström exponents (AE), seasons, SZAs, and scattering angles. The analysis results are also given to explain the different retrieval under various conditions of ASD and phase function. The DT method is applied to retrieve AHI AOD in Wuhan in order to reveal the different application effect of different retrieval methods. The AHI AOD, AHI DT AOD and MODIS aerosol product are all compared with CE-318 AOD.

### 3.1. Comparison of AOD between AHI and CE-318

An overall correlation analysis of AHI and CE-318 AOD is performed firstly. Fig. 2 presents the scatter plots of AHI and CE-318 AOD. The blue dashed line represents the 1:1 line, and the black dashed lines on both sides of the blue dashed line represent the envelopes of EE. A total of 2508 data pairs are left after the temporal-spatial matching and quality screening from three-year observations. The  $R^2$  value is 0.7, and approximately 48.80% of the samples are within the envelopes of expected error. In addition, the RMSE value is 0.17, and the density distribution of the samples shows that most AOD values are below 0.7. In sum, the AHI underestimates AOD in these three years.

Fig. 3a shows the variation of the bias between AHI and CE-318 AOD with the change of the latter. The bias is very close to 0 when the AOD is less than 0.2. The bias increases along with CE-318 AOD and reaches  $-0.4$  when the AOD is close to 1.4. Due to the small numbers of samples when AOD exceed 1.4, the bias show sharp fluctuations. However, AHI

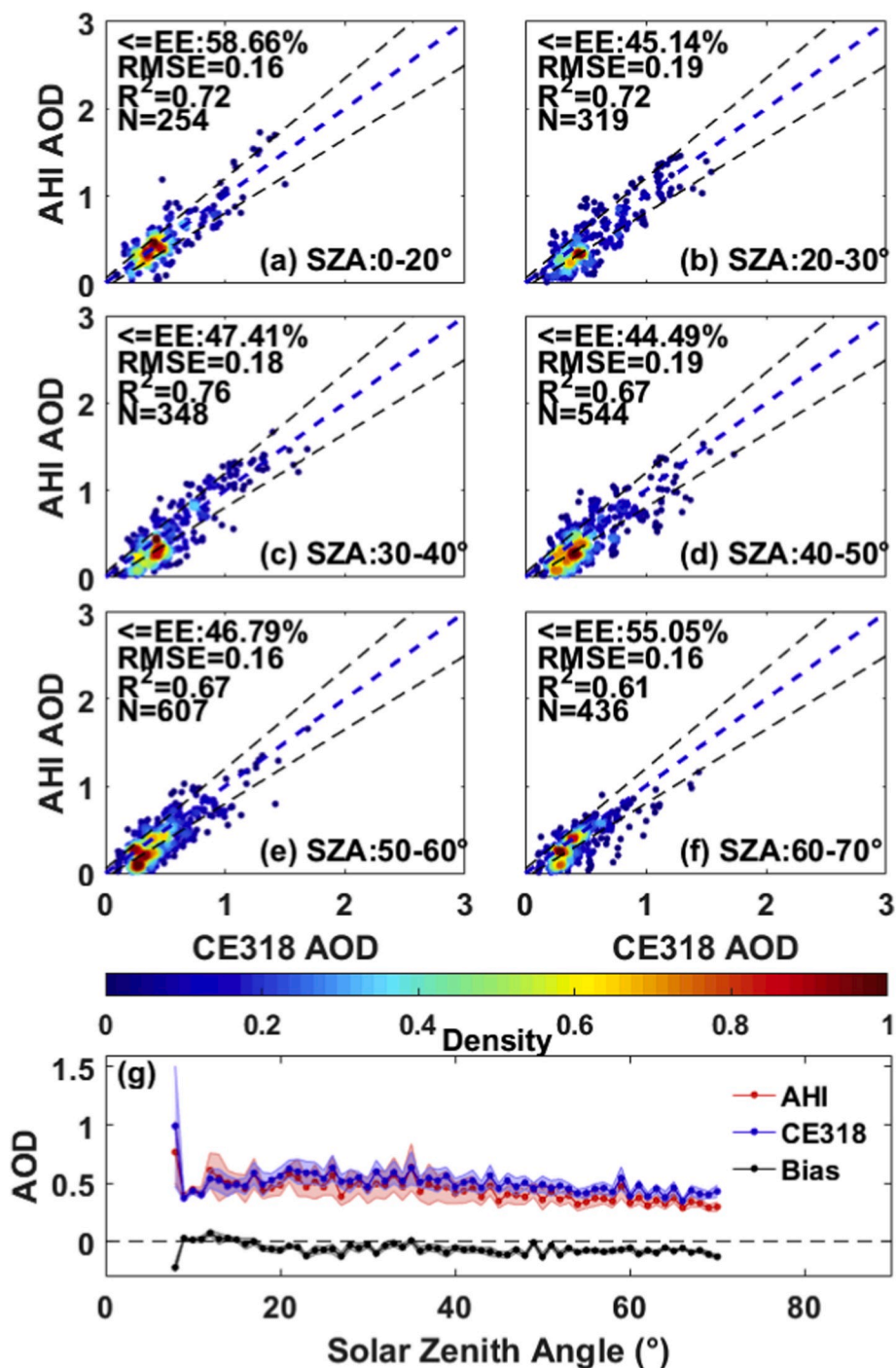


Fig. 8. Correlation analysis for all time AHI and CE-318 AOD while SZA is at (a) 0°–20°, (b) 20°–30°, (c) 30°–40°, (d) 40°–50°, (e) 50°–60°, and (f) 60°–70°. (g) Bias analysis between AHI AOD and CE-318 AOD relying on SZA.

performs a good retrieval when AOD range from 1.1 to 1.3, thereby indicating that AHI may have some advantages in retrieving AOD in this range of high AOD. In order to further discuss AHI aerosol retrieval under different aerosol load, we applied the DT method to perform comparison in section 3.5.

AE is an indicator that shows a negative correlation with aerosol size (Ångström, 1929). Fig. 3b shows the bias between AHI and CE-318 AOD while the AE (CE-318, 440 nm–675 nm) varies. The AHI AOD retrieval generates an overestimation with a decreasing trend when the AE is below 0.3. The bias is close to 0 when the AE range from 0.5 to 0.75. AHI underestimates AOD when the AE range from 0.8 to 1.7. The bias

changed barely when the AE range from 1 to 1.4, thereby suggesting a relatively stable deviation which reveals that AE within this range have little influence on AOD retrieval. When the AE exceed 1.6, the bias become closer to zero as the AE increase. The good estimation of AOD when AE is over 1.6 may relate to the good performance of Mie scattering algorithm with very small aerosol particles. We will discuss the influence of particle size on retrieval in the following section.

### 3.2. Seasonal analysis on AOD and ASD

Previous studies reveal that Wuhan suffers from high AOD

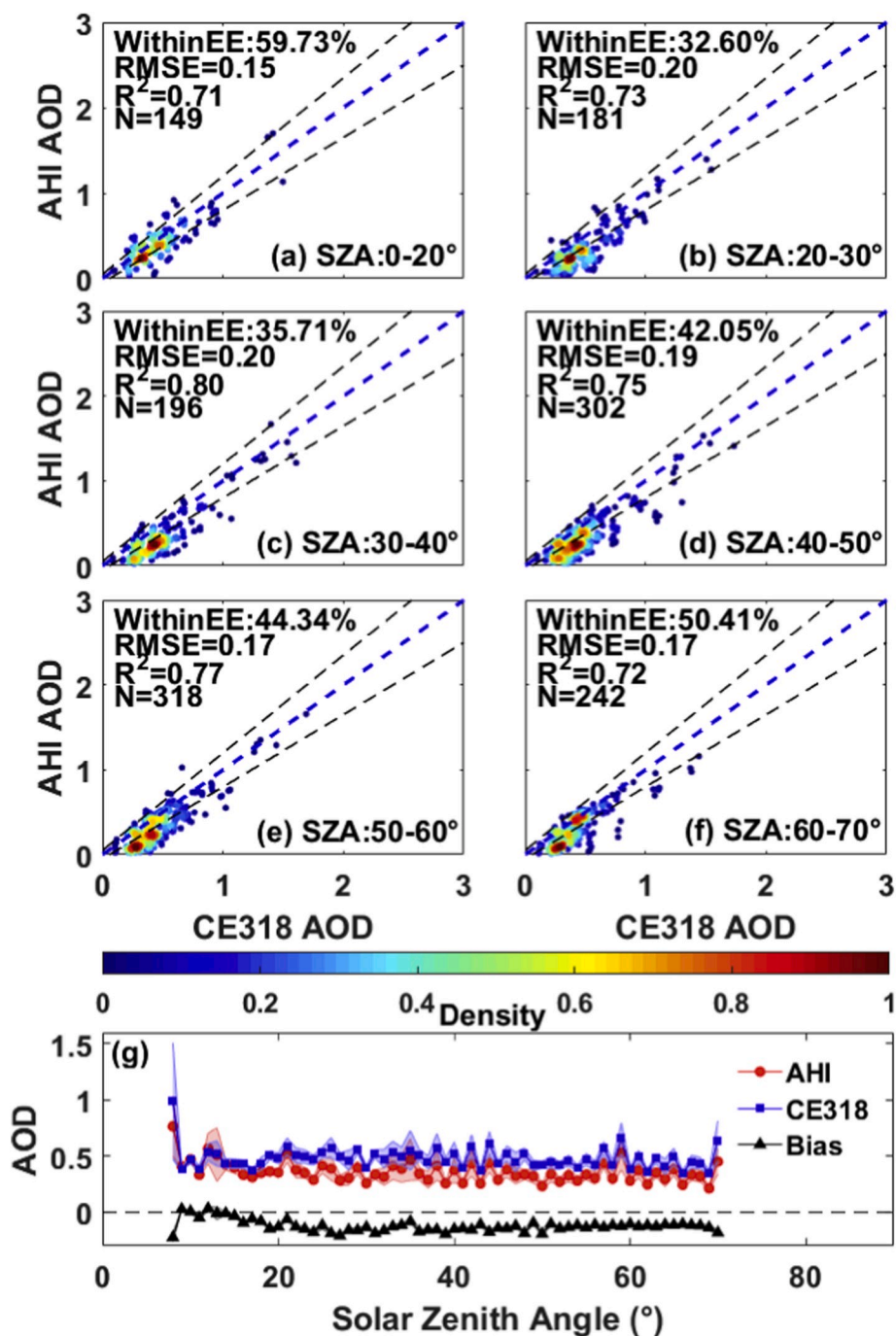


Fig. 9. Same with Fig. 8 but samples are limited in morning.

throughout a year, especially in spring and summer (Wang et al., 2015; Zhang et al., 2018). Aerosol types and their optical properties in this area vary with seasons. Northwest China has large arid and semi-arid regions that become main sources of aeolian dust aerosols in the atmosphere (Chooari et al., 2014; Wang et al., 2010, 2012; Ge et al., 2016). Dust events usually occur in spring, when dust is transported to downwind areas, including Wuhan (Wu et al., 2015) and shows great influence on cloud and precipitation (Huang et al., 2014). Wuhan has a subtropical monsoon climate and is full with rivers and lakes; rich moisture and rainfall promote hygroscopic growth of aerosol (Wang et al., 2015). In winter, frequent haze events occurred in recent years with transported and local aerosol (Xu et al., 2002; Zhang et al., 2018).

We make the seasonal analysis in order to analyze the influence that aerosol source, component or property may bring on retrieval. Fig. 4

presents the results of the correlation analysis across different seasons. AHI produces the best estimates in summer, when the  $R^2$  and RMSE values are 0.78 and 0.15, respectively. Approximately 58.12% of the samples are within the envelopes of EE. The largest number of matching samples is also recorded in summer. Spring and autumn have similar numbers of samples but show different estimation effects. Specifically, the  $R^2$  and RMSE values in spring are 0.76 and 0.17, respectively, whereas those in autumn are 0.46 and 0.21. Huge differences are also observed in the percentage of samples within EE, that is, around 49.71% and 34.76% of the samples are within the EE in spring and autumn, respectively. The limited number of samples in winter can be ascribed to the continuous cloudy or rainy weather and thick haze in the area. According to meteorological data, only 34.6% of the winter days in Wuhan over the past three years are sunny. Moreover, given that the planetary

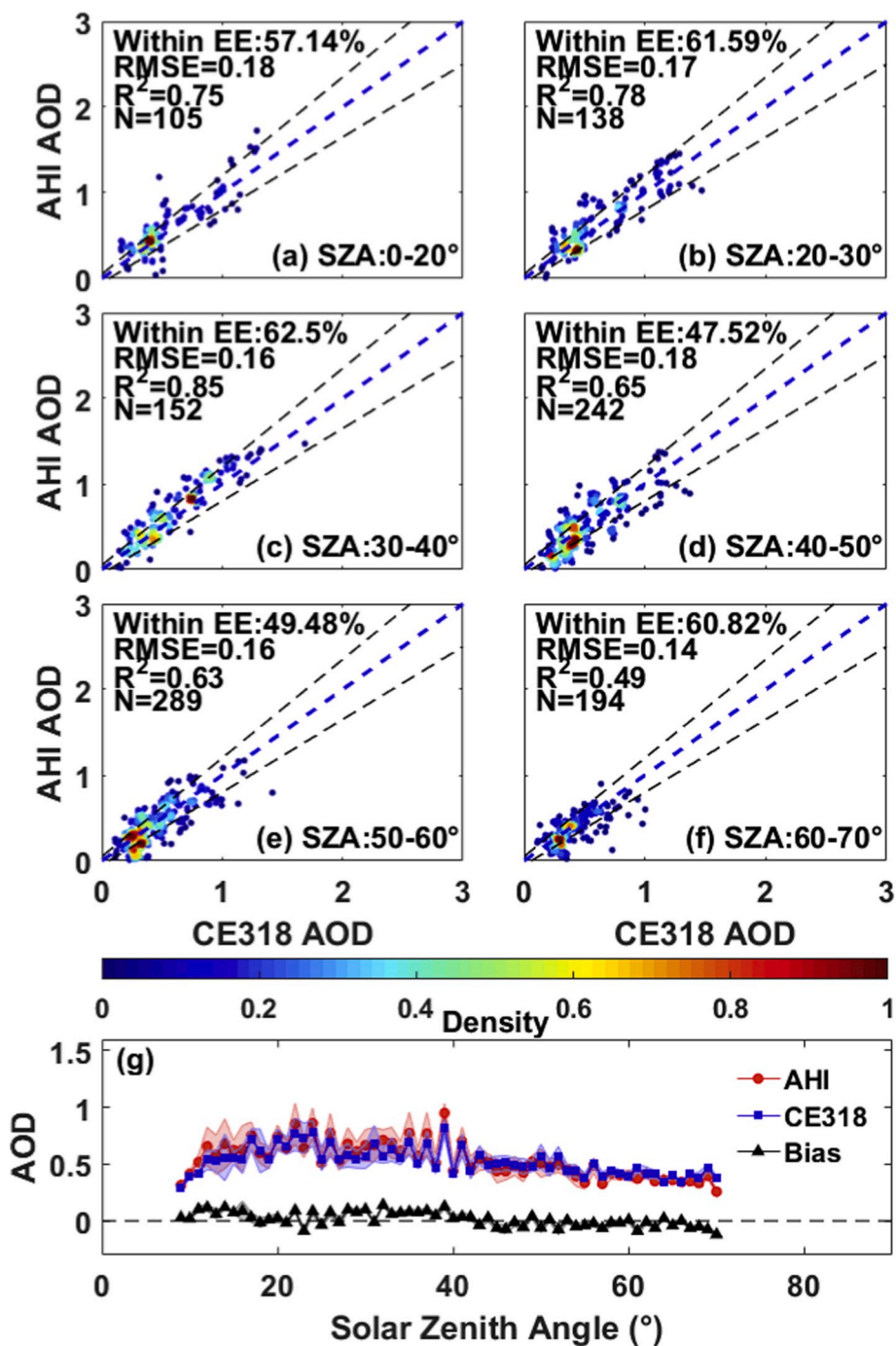


Fig. 10. Same with Fig. 8 but samples are limited in afternoon.

boundary layer is low in winter, even the Lidar in the station cannot break through the thick cloud and haze in most days (Liu et al., 2018a, b). In sum, CE-318 can hardly record effective observations during this period. The 66 samples collected in winter have  $R^2$  and RMSE values of 0.42 and 0.21, respectively, and 16.67% of these samples are within the envelopes of EE. Samples below EE are obviously more than that upon EE in all the seasons, indicating an underestimation all over the year.

Fig. 5 presents a histogram of the appearance frequency of bias between CE-318 and AHI AOD. The blue line represents the fitting normal distribution curve. The best mean value ( $-0.04$ ) is recorded in summer with an accompanying standard deviation (std) of 0.19. Meanwhile, the fitting normal distribution curve for spring has mean and std values of  $-0.09$  and 0.19, whereas that for autumn has mean and std values of

$-0.13$  and 0.23, respectively. These statistics are comparable but somewhat larger than the computus of MODIS AOD (Anderson et al., 2013). Winter shows the worst mean bias ( $-0.21$ ). The findings in Fig. 5 are similar to those in Fig. 4, which means the AHI AOD minus CE-318 AOD mean biases in summer and spring are closer to zero compared with that in autumn and winter.

ASD plays an important role in aerosol retrieval as determining aerosol optical properties (Tegen and Lacis, 1996). The volume median radius for the fine and coarse modes are set to 0.143 and 2.834  $\mu\text{m}$  in AHI aerosol algorithm (Yoshida et al., 2018). For fine-mode particle, Mie scattering algorithm is used to simulate extinction and scattering properties in AHI aerosol algorithm. AHI adopts the coarse dust model of Omar et al. (2005) and uses non-spherical parameters based on the

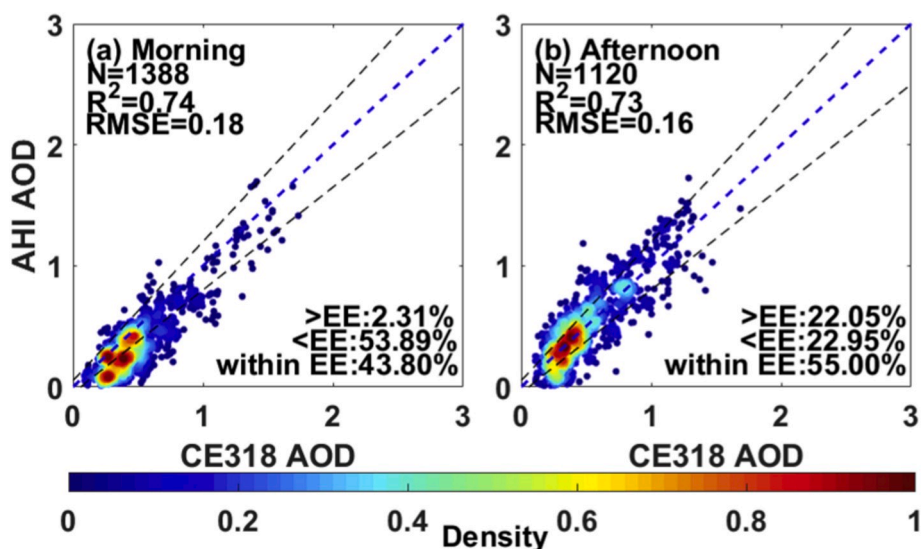


Fig. 11. Correlation analysis of AHI and CE-318 AOD in the morning and afternoon. 53.89% of the sample are below EE in the morning, and 22.95% are below EE in the afternoon. The local time of 12:00 (corresponding to about 12:30 in Beijing time) is used to distinguish morning and afternoon.

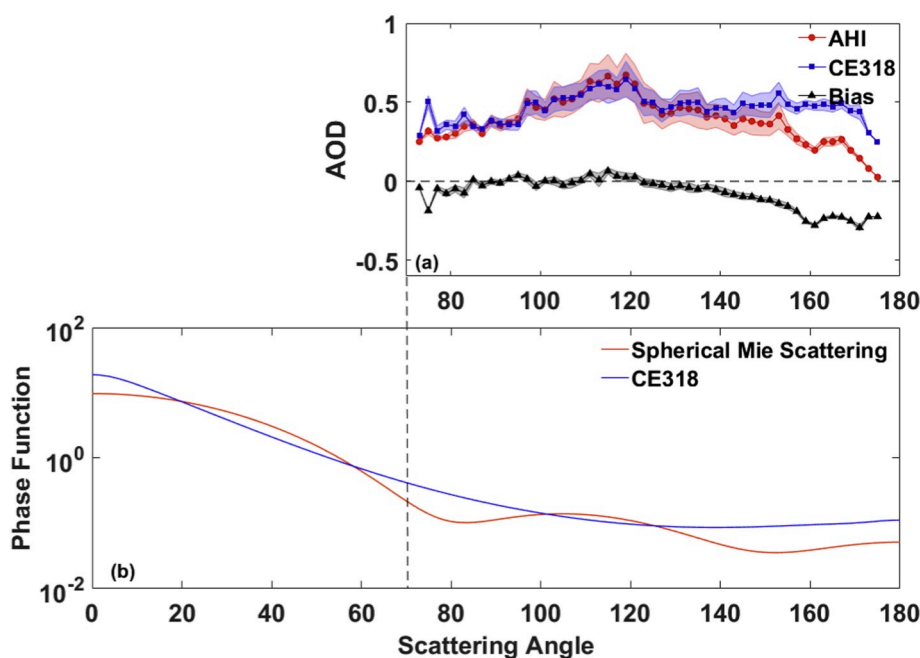


Fig. 12. (a) Variation of AHI (red circle and line) and CE-318 AOD (blue circle and line) as well as their bias (AHI minus CE-318, black circle and line) at different scattering angles. (b) The phase function simulated by the spherical Mie scattering function using CE-318 fine-mode effective radius and complex refractive (red line), and the CE-318 simulated phase function (blue line). (For interpretation of the references to color in this figure legend, the reader is referred to the Web version of this article.)

semi-empirical theory of Pollack and Cuzzi (1980). According to Nakajima et al. (1989), the non-spherical model is constructed referring to the observations in dust events of East Asian and it performs well in this region. Here we present the ASD that provided by CE-318 under different seasons, and make comparison with what AHI simulates. Considering that the coarse-mode simulation method is based on the observation and performs well in East Asia, we focus on the fine-mode simulation and paint the efficiencies and factors that varies along with size parameter ( $x$ ) according to Mie scattering algorithm. The size parameter is calculated by  $2\pi \times \text{radius}/\text{wavelength}$  and it is widely used in Mie scattering calculation to present size.

Fig. 6a presents the seasonal aerosol size distribution observed by CE-318 in Wuhan. The black lines denote the default AHI-set median radiuses of fine- and coarse-mode particles. The concentration of coarse-mode aerosol are higher in spring and winter, and their volume median radius are lower than summer and autumn. The median radius of the

coarse-mode particles during spring is close to the default value. The well-simulated coarse-mode model may explain why better retrieval results are obtained in spring than in autumn. The volume medium radius set by AHI for fine-mode particles is obviously lower than what has been observed in all the seasons, and AHI also underestimates the fine-mode effective radius as the effective radius is calculated by integrating size distribution. Fig. 6b presents the variances in single scattering albedo and asymmetry of fine-mode particle along with size parameter while Fig. 6c presents two phase functions simulated by using AHI effective radius and CE-318 annual effective radius. The underestimation of fine-mode effective radius slightly decrease single scattering albedo but obviously increase backscattering (according to lower asymmetry and higher phase function over scattering angle of  $90^\circ$ ) as Fig. 6b and c presents, which in turn may increase path reflection. Moreover, the overestimation of path reflection would underestimate the AOD in AHI according to Yoshida et al. (2018), fitting the result of

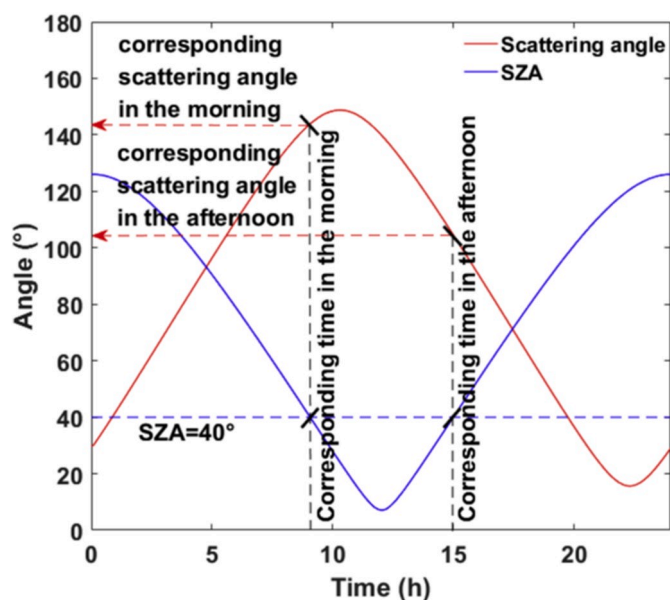


Fig. 13. Variation of scattering angle (red) and SZA (blue) across hours of local time in June 23rd Wuhan. The dashed lines respectively represent  $SZA = 40^\circ$  (blue), corresponding time in the morning and afternoon (black), and their corresponding scattering angles (red). These dashed lines are used to indicate the same SZA correspond to different scattering angle in morning and afternoon. (For interpretation of the references to color in this figure legend, the reader is referred to the Web version of this article.)

comparison. So the low default medium radius of fine-mode particles may be among the reasons for the underestimation of AOD.

The aerosol hygroscopic growth in summer and autumn may also contribute to the underestimation of AOD. Wang and Martin (2007) conducted a theoretical study and showed that the hygroscopic growth can affect the retrieval of not only AOD but also its wavelength dependence; the decrease of backscattering and increase of single scattering albedo associated with the particle size growth in high relative humidity conditions can have the opposite effect on urban AOD retrieval. However, if aerosol particles are highly scattering, the hygroscopic growth that is not considered in the retrieval algorithm will lead to underestimate of AOD (Wang and Martin, 2007), which is consistent with the analysis with Fig. 6. Specifically, for urban areas like Wuhan, aerosol hygroscopic growth contributes to the increase of aerosol fine-mode particle radius (Che et al., 2015). Zhang et al. (2017a,b) also indicates that aerosol hygroscopic growth increase the forward scattering and decrease the backward scattering. So neglecting the hygroscopic growth would contribute to the AOD underestimation by overestimating path reflection. The worst retrieval effect is recorded in winter. Zhang et al. (2018) argued that the volume median radius of fine-mode particles can be as large as  $0.194 \mu\text{m}$  during a haze event in winter. The volume median radius of fine-mode particles is much larger than what has been set by AHI, thereby contributing to obvious underestimations of AOD in winter. Overall, the underestimation of particle size is an important reason for AHI's underestimation of AOD throughout the year.

The 10-min temporal resolution of AHI AOD allows diurnal analysis. We provide bias variations of AOD in four seasons and the whole year to reveal the different retrieval throughout a day. In spring (Fig. 7a), the AOD increases, fluctuates, and reaches its peak at about 14:30. Although AOD briefly increases at 16:00, the overall trend is decreasing after 14:30. The variation of bias is similar with AOD in spring. The AOD in summer (Fig. 7b) is almost constant from 8:00 to noon, and a slight increase is observed from 12:00 to 13:30. The AOD peaks at 13:30 before a sharp decrease. After 14:00, the AOD increases and then decreases. The bias is close to zero and remains stable in the morning, fluctuates, and then declines along with time in the afternoon. The diurnal

variation of AOD in autumn (Fig. 7c) is very complex. Specifically, the lowest and highest AOD are observed at about 9:00 and 12:00, respectively. The bias indicates an underestimation almost in the day. Given the small sample numbers, the figure of winter (Fig. 7d) does not present a continuous curve for the variation of AOD in the day. The peak appears at about 12:30, and the bias is close to zero from 10:00 to 11:00. As shown in Figure 7e, 3-year averaged AOD slowly increases from sunrise to about 15:00 and then declines rapidly from 15:00 to sunset. This diurnal variation of AOD is similar with observation for inland urban areas presented by Lennartson et al. (2018), and the most negative values all occur near the midday. The bias is closer to zero in the afternoon than in the morning, and AHI is often underestimated AOD before noon. Fig. 7 reveals that the bias of AHI retrieval may have obvious difference in a day. As angles like SZA, and scattering angle may be able to influence the retrieval and vary with time, we then discuss these angles and analyze their influence on AHI retrieval in the following section.

### 3.3. Effect of SZAs on AOD inversion

The SZA which has a direct effect on atmospheric path radiation, further influence the AOD retrieval (Levy et al., 2013). SZAs vary along with time in a day, and AHI carried by a geostationary satellite retrieves AOD under varying SZAs. The radiative transfer model which is used to retrieve AOD from satellite observations usually simplifies the calculation of multiple scattering. Larger SZAs cause the solar radiation to travel longer atmosphere path and interact with more aerosol particles, and more scattering process simulations of aerosol particles may induce higher estimation error. The variation of SZAs may partly explain the diurnal bias variation of AHI retrieved AOD.

Here we provide correlation and bias analysis for AHI AOD under different SZAs in order to discuss the influence of SZA on AHI retrieval. Fig. 8a–f shows that the variation of  $R^2$  overall shows a fluctuating decreasing trend along with an increasing SZA, but an obvious inflection point is observed when the SZAs range from  $30^\circ$  to  $40^\circ$ . The best  $R^2$  appears at  $30^\circ$ – $40^\circ$  with  $R^2$  and RMSE values of 0.76 and 0.18, respectively, and with around 47.41% of samples within EE. The worst  $R^2$  is observed at SZA of  $60^\circ$ – $70^\circ$ . Relatively low RMSE values (about 0.16) are recorded from  $0^\circ$  to  $20^\circ$  and from  $50^\circ$  to  $70^\circ$ . While SZAs range from  $20^\circ$  to  $50^\circ$ , the RMSE values are about 0.18. More than 55% of the samples are within EE at SZAs of  $0^\circ$ – $20^\circ$  and  $60^\circ$ – $70^\circ$ , whereas about 45% are within EE at the other SZAs. Fig. 8g shows the variation of AHI AOD, CE-318 AOD and their bias (AHI minus CE-318) relying on SZAs. AHI underestimates the AOD at most situations. The bias comes near zero only at an SZA of  $10^\circ$ – $20^\circ$  or about  $35^\circ$ .

The SZA is symmetric at noon of local time, so the overall analysis of SZA that Fig. 8 presents is unable to reflect the difference between the morning and afternoon. Here we separately discuss the influence of SZA on AHI AOD retrieval in these two periods. Fig. 9a–f presents the results of the correlation analysis for the AHI AOD retrieval relying on SZAs in the morning. The  $R^2$  value reaches its peak (0.8) when SZAs range from  $30^\circ$  to  $40^\circ$  and exceeds 0.7 at all other SZAs. Meanwhile, the RMSE values range from 0.15 to 0.17 at SZAs of  $0^\circ$ – $20^\circ$  and  $50^\circ$ – $70^\circ$ , and turn to be around 0.2 at other SZAs. Around 59.73% of the samples are within EE at SZAs of  $0^\circ$ – $20^\circ$ , range from 30% to 50% at other SZAs, and increase along with SZAs. Fig. 9g shows the bias variation between AHI and CE-318 AOD in the morning. AHI underestimates AOD at most SZAs except from  $10^\circ$  to  $15^\circ$ . The correlation analysis for the afternoon (Fig. 10a–f) reveals that  $R^2$  initially increases and then decreases as the SZA increases. The  $R^2$  values reach the peak (0.85) at SZAs of  $30^\circ$ – $40^\circ$ , and low RMSE values (around 0.15) are recorded at SZAs of  $30^\circ$ – $40^\circ$  and  $50^\circ$ – $70^\circ$ . Below 50% of the samples are within EE at SZAs of  $40^\circ$ – $60^\circ$ . Fig. 10g shows that the bias (AHI minus CE-318) are near zero when the SZAs are around  $20^\circ$  or above  $40^\circ$ . Comparing the correlation analysis in morning and afternoon at different SZAs, we find that the morning has higher  $R^2$  than the afternoon when SZAs higher than  $40^\circ$ , while the

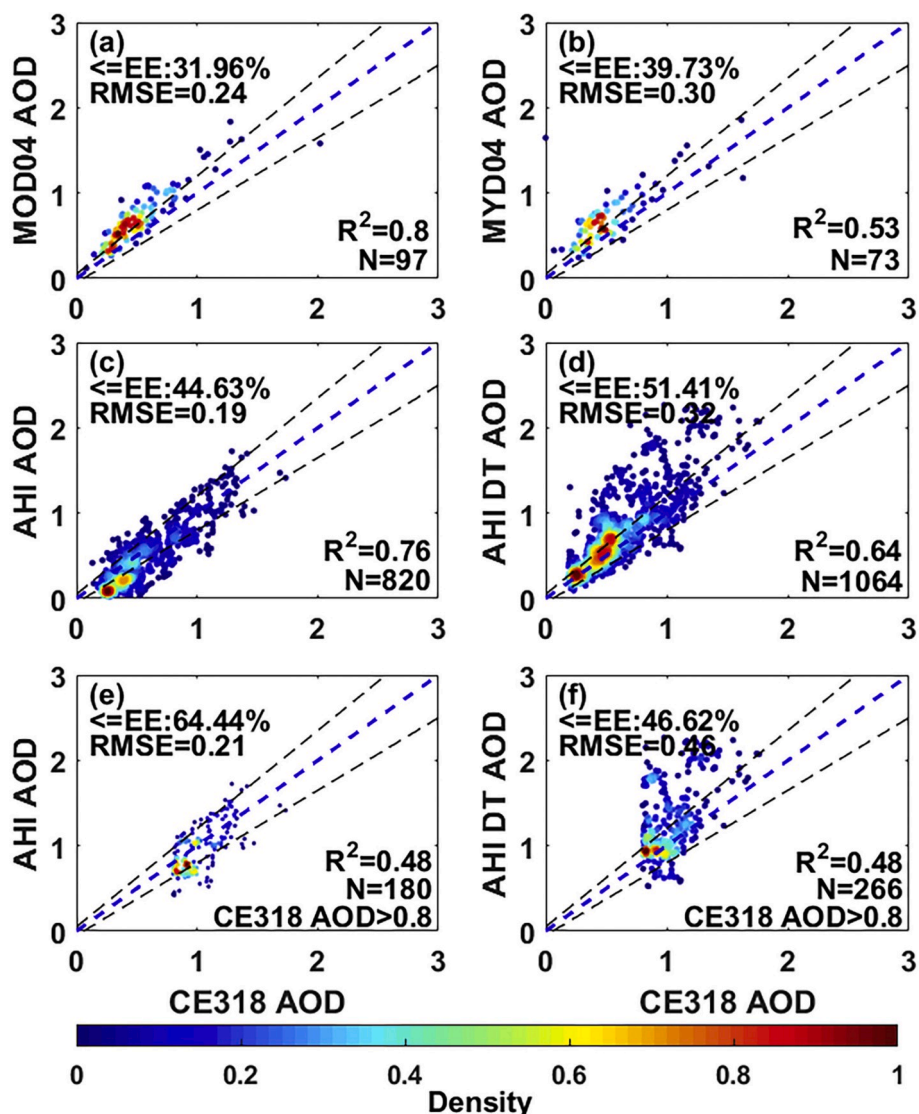


Fig. 14. Correlation analysis for (a) MODIS MOD04 AOD, (b) MODIS MYD04 AOD, (c) AHI AOD, and (d) AHI DT AOD retrieval result from AHI level 1 data by comparing with CE-318 500 nm AOD in 2016, Wuhan. Choose the CE-318 AOD which more than 0.8, and compare it with the corresponding AHI AOD (e), and the AHI DT AOD (f).

afternoon gets better  $R^2$  than the morning when SZA lower than  $40^\circ$ . We attribute this phenomenon to the influence of scattering angle which will be explained in detail in section 3.4. For percent within EE and RMSE, the afternoon performs better at all SZAs except  $0-20^\circ$ . The bias analysis for Figs. 9g and 10g present that the morning has an overall underestimation while the bias in afternoon wave around zero. These results indicate a better retrieval in the afternoon, and the different retrieval at same ranges of SZAs reveals that there are other factors deeply affect AHI retrieval. In order to present the difference of retrieval in morning and afternoon directly, we provide correlation analysis for the morning and afternoon in Fig. 11.

As mentioned above, the SZA is symmetric at around noon. If SZAs affect AHI retrieval independently, the correlation analysis would not show great difference in morning and afternoon. In order to further discuss the influence of SZAs on AHI retrieval. We examine the AHI AOD distinguishing the morning and afternoon in Fig. 11. The  $R^2$  and RMSE values in the morning are 0.74 and 0.18, respectively, while those in the afternoon are 0.73 and 0.16, indicating that AOD of AHI has similar correlation but smaller bias with CE-318 in the afternoon than in the morning. About 43.80% of the samples are within EE in the morning, while 55% are within EE in the afternoon. A similar percentages of

samples below and above EE is observed in the afternoon (23% and 22%, respectively), whereas 54% of the samples are below EE in the morning. The big difference of percent below and above EE in the morning may reveal a stable underestimation of AOD during the time while the result in the afternoon reveals a much better retrieval. Overall, the correlation analysis in the morning and afternoon shows a little bit difference in  $R^2$  and RMSE, but a great difference in EE. The result reveals other factors like scattering angle affect retrieval and lead to the underestimation of AHI AOD, so we will discuss the influence from scattering angle and phase function in the following section.

### 3.4. Extensive discussion of SZA, scattering angle and phase function

The scattering angle is calculated by using SZA, satellite zenith angle (fixed value for the same location in AHI retrieval) and relative azimuth angle as shown in formula (2.4.2). The scattering angle participates in radiation calculation in the scattering part through the phase function, and the phase function describes the angular distribution of radiation scattering (Kokhanovsky, 2009). Yoshida et al. (2018) revealed that the bias of retrieval varied under different scattering angles, which could be ascribed to the misfit of aerosol models. As an important parameter in

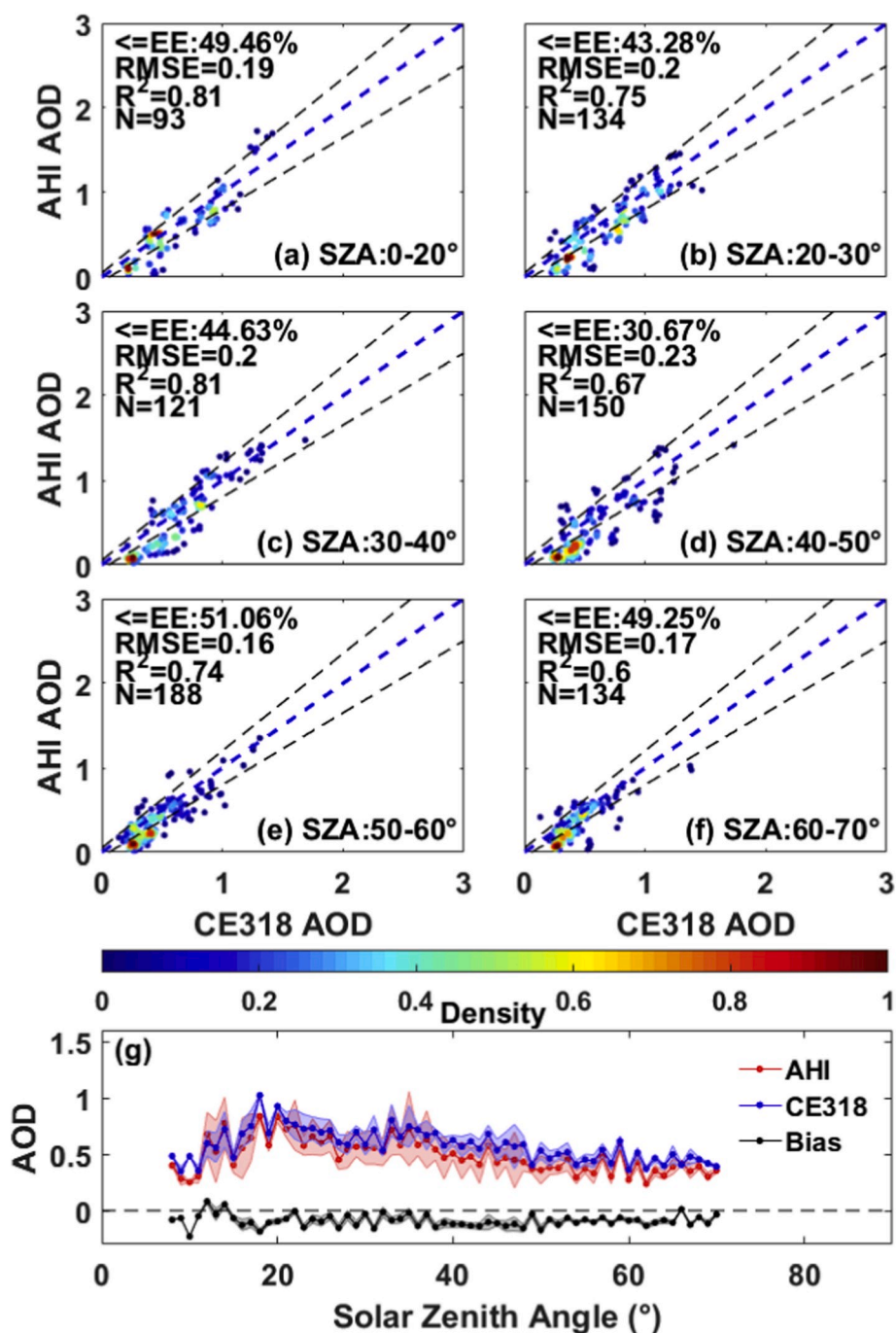


**Fig. 15.** Correlation analysis of AHI AOD and CE-318 AOD in 2016 while the SZA ranges from (a) 0°–20°, (b) 20°–30°, (c) 30°–40°, (d) 40°–50°, (e) 50°–60°, and (f) 60°–70°. (g) Variation of bias (AHI minus CE-318) relying on SZA.

AHI aerosol model, phase function simulated by spherical Mie scattering algorithm can be related to the variation of AOD bias (AHI minus CE-318) relying on scattering angle. Fig. 12a shows AHI underestimates AOD when the scattering angle is below 90°. When the scattering angle is between 100° and 120°, AHI overestimates AOD slightly. After that, underestimates occur and enlarge with the increase of scattering angles.

Scattering angles affect retrieval through phase function. AHI uses the spherical Mie scattering function to simulate the phase function of a fine-mode particle (Yoshida et al., 2018). In this paper, we only discuss the simulation of phase function of fine-mode particles because AHI employs a semi-empirical theory to simulate the phase function of coarse-mode particles, and the simulated phase function for coarse-mode shows a good fit with observations in East Asian according

to the study of Nakajima et al. (1989). Xu and Wang (2015) has mentioned that the aerosol particle size distribution can be well characterized with an effective radius, so we use a fine-mode effective radius and a complex refractive index observed by CE-318 to calculate the phase function through spherical Mie scattering function, and then make comparison with the fine-mode phase function from CE-318 to analyze the error that spherical Mie scattering algorithm brings on phase function simulation, and the results are presented in Fig. 12b. It should be noted that CE-318 does not provide phase function at 500 nm, so we use the phase function at 440 nm instead. As can be seen in this figure, when the scattering angle is between 80° and 100°, the Mie scattering algorithm which AHI used underestimates the phase function. Spherical Mie scattering algorithm overestimates the phase function when the

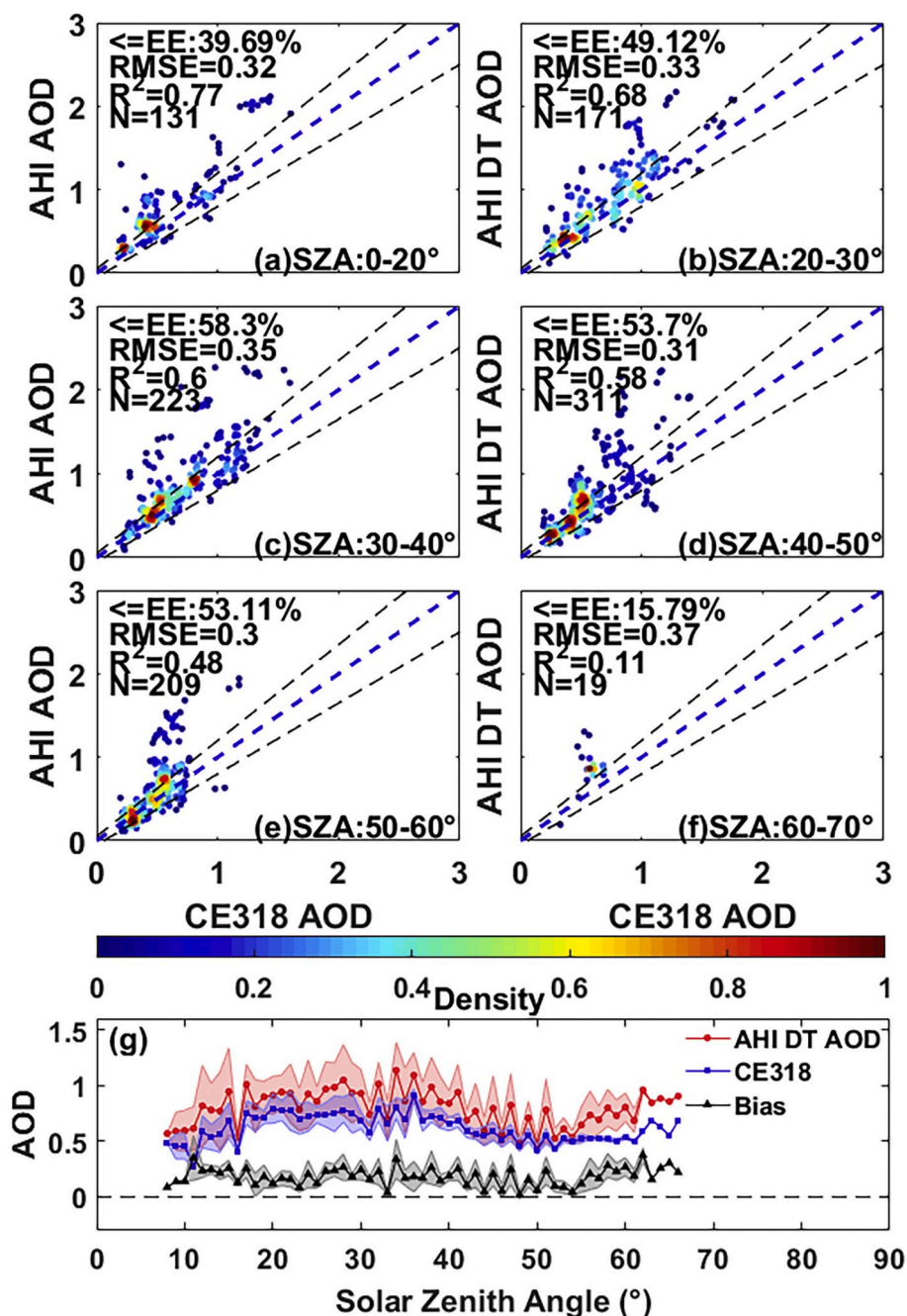


Fig. 16. Same as Fig. 15 but the comparison is between AHI DT AOD and CE-318 AOD in 2016.

scattering angle ranges between  $100^\circ$  and near  $125^\circ$ , and the biggest overestimation appears at a scattering angle of about  $115^\circ$ . The variation of difference between the Mie scattering algorithm simulated phase function and the phase function derived from CE-318 observations are almost uniformly fitted with the trend of bias shown in Fig. 12a. Therefore, how the AHI aerosol algorithm simulates the fine-mode particle phase function closely relates to the bias of the retrieved AOD.

As mentioned above, The SZA participates in calculating scattering angle which means these two angles are related and combine to affect retrieval. Here we paint the variation of SZA and scattering angle with time in Fig. 13 to explain that the same SZA corresponds to different scattering angle in morning and afternoon, and further explain why correlation analysis under same SZAs show such a difference in morning and afternoon by considering the influence of scattering angle. From Fig. 13, scattering angle initially increases before decreasing while SZA

firstly decrease and then increase during daytime of June 23rd. The peak of scattering angle is observed at about 10:15 (local time) in Wuhan, while the lowest SZA appears at 12:00 (local time). As Fig. 13 shows, in June 23rd when SZA come to be  $40^\circ$  (blue dashed line), the corresponding time (black dashed line) turns to be 9 o'clock and 15 o'clock in morning and afternoon respectively, and the corresponding scattering angle (red dashed line) turns to be  $145^\circ$  and  $105^\circ$  in morning and afternoon respectively. So we proved that same SZA corresponds to different scattering angle in morning and afternoon. Then if the SZA increases from  $40^\circ$ , the corresponding scattering angle would decrease from  $145^\circ$  to  $105^\circ$  in morning and afternoon as Fig. 13 shows. According to Fig. 12a, if scattering angle decreases from  $145^\circ$ , we can find the retrieval may become better as scattering angle is between  $100^\circ$  and  $125^\circ$ , while it decreases from  $105^\circ$ , the retrieval can only get worse. This phenomenon could explain the conclusion that we have presented in

section 3.3, which is the  $R^2$  between AHI and CE-318 AOD are higher in the morning than in the afternoon when SZA higher than  $40^\circ$ . The analysis above is based on date of June 23rd. In other date, variation with time of these two angles have same variation trend, same time of highest value and lowest value. The only difference is that curves for SZA and scattering angle would up shift in other date compared with June 23rd, leading to higher corresponding scattering angle both in morning and afternoon when SZA comes to  $40^\circ$ . The difference would not influence our conclusion, so we only take the June 23rd as an example. It is obvious to see that the scattering angle is one of that cause for the difference in morning and afternoon, and SZA and scattering angle combine to affect retrieval.

### 3.5. Differences between DT and AHI official retrieval algorithms

We retrieved the AOD from AHI level 1 data by applying the DT method (Ge et al., 2019; Levy et al., 2010), then compared the MODIS AOD, AHI AOD and AHI DT AOD with the CE-318 AOD. Fig. 14a and b shows that the AOD from MOD04 has a higher  $R^2$  (0.80) compared with MYD04 (0.53). About 32% and 40% of the MOD04 and MYD04 samples are within EE. These two comparisons show that MOD04 has better performance in Wuhan comparing with MYD04. As shown in Fig. 14c, the AHI AOD has a lower  $R^2$  (0.76) compared with MODIS MOD04 AOD yet has more samples (44.6%) within EE. Meanwhile, the AHI DT AOD (Fig. 14d) shows a similar RMSE with MODIS MYD04 yet demonstrates a worse retrieval effect when compared with AHI AOD (lower  $R^2$ , similar percentage of samples within EE, and higher RMSE).

As the AHI AOD performs better in Wuhan than MOD04, MYD04 and AHI DT AOD, we try to give some explanation. First, we consider the influence of aerosol loading. The DT method usually demonstrates a poor retrieval effect at AOD more than 0.8, indicating a relatively higher uncertainty under heavy aerosol loading (Liu et al., 2014a,b, 2018). So we limit the CE-318 AOD that values must be higher than 0.8 in Fig. 14e and f, and make comparison with corresponding AHI AOD and AHI DT AOD to show the difference under heavy aerosol loading. Both AHI and the dark target method show a different performance after limiting AOD (lower  $R^2$  but higher percent within EE). The AHI DT AOD shows a high RMSE of 0.46 with CE-318 AOD, whereas the AHI AOD has a RMSE of 0.21 with CE-318 AOD after limitation. It suggests that AHI aerosol retrieval algorithm has some advantages in retrieving AOD in Wuhan at periods under heavy aerosol loading comparing to the DT method, this result is consistent with the result with Tao et al. (2017b). Gupta et al. (2019) also revealed that the DT method would overestimate AHI AOD. The cloud detection method applied by AHI is described in Ishida and Nakajima (2009) and may explain the advantage of AHI retrieval under heavy aerosol loading. This method shows advantages in detecting areas with ambiguous cloudy conditions, and Wuhan are often cloudy. So this method may be more suitable in Wuhan than the MODIS C006-L cloud mask method applied on the DT method, thereby explaining why the AHI shows a better retrieval performance compared with the DT method. Another reason may be the difference of aerosol models that AHI aerosol algorithm and the DT method take. AHI uses a look-up table, two default volume median radiuses, and spherical and non-spherical scattering methods to construct an aerosol model (Yoshida et al., 2018) instead of using those aerosol models constructed via a cluster analysis of ground-based measurements (Omar et al., 2005; Levy et al., 2007a). Given the lack of ground-based observations in Central China, the aerosol models constructed via cluster analysis cannot cover the characteristics of aerosols in Wuhan, and the estimation of single scattering albedo also brings error, thereby explaining the poor retrieval results of the DT method. Although the default volume median radius of AHI's aerosol model does not exactly fit the observations, the look-up table can, to some degree, correct the final simulated size distribution through looking up for suitable fine-mode fraction. The AHI aerosol algorithm may show a better performance in areas where adequate aerosol prior knowledge is lacking and may have better retrieval AOD.

Surface reflectance estimation and aerosol model are two main error source in the DT method. However, Jin et al. (2019) found aerosol models were main reason to cause the MODIS C6.1 retrieval errors in Wuhan. And our work aims more on impacts of angles or size distributions on AHI AOD retrieval, separately considering surface reflectance for the DT method may make section 3.5 too long and it will take our article deviate from the core theme, so we would not talk about the influence of surface reflectance and it would not affect our conclusion.

AHI aerosol algorithm and the DT method perform differently in retrieving AHI AOD. We here make correlation and bias analysis of AHI AOD and AHI DT AOD comparing with CE-318 AOD, discussing SZA's influence on retrieving AOD from these two methods. From Figs. 15 and 16, the highest  $R^2$  for the AOD of these two methods with that of CE-318 appear at SZAs ranging from 0 to  $20^\circ$ , whereas the lowest  $R^2$  values of AHI AOD and AHI DT AOD are observed at SZAs ranging from  $60$  to  $70^\circ$ . AHI AOD shows smaller variations (0.60–0.81) in its  $R^2$  when the SZA ranges from  $20^\circ$  to  $70^\circ$  compared with AHI DT AOD (0.11–0.77). This result indicates that in the DT method, SZA has large effect on retrieval. Figs. 15g and 16g show that the AHI AOD are lower than CE-318 AOD at most SZAs, whereas AHI DT AOD are higher than CE-318 AOD. The bias of the AHI AOD and CE-318 AOD is near to zero when SZA is at about  $10^\circ$ , and the largest bias appear when SZAs range from  $40$  to  $50^\circ$ . The bias between AHI DT AOD and CE-318 AOD shows a similar trend as CE-318 AOD varies, which may suggest that the DT inversion is influenced by aerosol concentration to some extent.

## 4. Conclusion

The AOD provided by AHI which carried by a geostationary meteorological satellite has great advantages in temporal resolution, and has wide application such as aerosol short-term change tracking (Yoshida et al., 2018). In order to ensure its regional reliability and improve the application effect of AHI AOD, it is necessary to verify and analyze its data product as well as search for the factors that bring negative effect on retrieval. In this study, we obtain AOD from a well-maintained CE-318 sun photometer in Wuhan as the standard data, through comparing with the high temporal resolution AHI aerosol product, we completed the all-around and detailed evaluation for AHI AOD in Central China.

The AHI AOD shows a good  $R^2$  of 0.7, but much more samples are below EE rather than above, which reveals that AHI overall underestimates AOD in Wuhan. Bias (AHI minus CE-318) analysis under different AOD and AE shows AHI aerosol algorithm performs better at very low aerosol loading (AOD<0.2) or for very small particles (AE>1.6). As aerosol optical properties varies with seasons, we perform correlation analysis for seasons and attribute the difference of retrieval to the simulation of ASD. AHI aerosol algorithm uses default fine- and coarse-mode volume medium radius to simulate ASD but the observed volume medium radius are different in seasons, which causes the different retrieval in seasons. Fine-mode ASD contributes more to the seasonal difference as it always dominates, so we present how the fine-mode radius affects scattering base on spherical Mie scattering method which is used by AHI aerosol algorithm for fine-mode particle. These works help us to prove that the lower default fine-mode volume medium radius causes the overestimation of back-scattering, which finally leads to the underestimation of AHI AOD. Then the influence of SZA on AHI aerosol retrieving is discussed. AHI aerosol algorithm shows best performance when SZA ranges from  $30^\circ$  to  $40^\circ$ . SZA is symmetric with noon but the diurnal has shown difference in retrieval between morning and afternoon, so we give correlation and bias analysis relying on SZA respectively in morning and afternoon. The difference between morning and afternoon indicates that there are other factors affect retrieval. To test whether scattering angle is the factor that affects retrieval combining with SZA, bias analysis for AHI and CE-318 AOD relying on scattering angle is performed. Scattering angle affects retrieval through phase function, so we also simulated the phase function through

spherical Mie scattering method to compare with CE-318 observed phase function in order to evaluate the error that Mie scattering method brings to phase function simulation. We find that the variation of the difference between simulated phase function and CE-318 observed phase function is uniformly fitted with the trend of bias between AHI and CE-318 AOD. It proves that scattering angle greatly affects AHI aerosol retrieval through phase function. Then we relate the SZA and scattering angle through time, showing that same SZAs corresponds to different scattering angle in morning and afternoon, and we prove that scattering angle is an important reason that causes the different retrieval under same SZA in morning and afternoon. At last, we use the DT method to retrieval AHI AOD in 2016 of Wuhan and provide comparison. MODIS MOD04 and MYD04 aerosol product are also involved into the comparison. AHI AOD performs better than AHI DT AOD, MOD04 and MYD04 AOD in Wuhan. The good performance may relate to the cloud detecting method and aerosol model that AHI aerosol algorithm uses as Wuhan has frequent cloudy weather, heavy aerosol loading, and is lack of prior information of aerosol properties.

Our analysis for AHI AOD and CE-318 AOD could also be performed in other areas, and may help us to further understand the influence of aerosol model (ASD, phase function) on AHI retrieving. But in this work, data from a single area could partly prevent some disturbance such as surface reflectance and satellite zenith angle when analyzing the influence of SZA or scattering angle on retrieval, so in this study, we only chose the ground-based observation from the Wuhan University atmospheric observation station. In the future, as more AERONET sites observation will be introduced, through classifying aerosol and obtaining suitable volume medium radius in AHI aerosol algorithm, AHI AOD retrieval would be improved.

#### Declaration of competing interest

The authors declare that they have no conflict of interest.

#### CRedit authorship contribution statement

**Ming Zhang:** Conceptualization, Methodology, Investigation, Writing - review & editing. **Yingying Ma:** Validation, Formal analysis, Visualization, Writing - review & editing. **Yifan Shi:** Validation, Formal analysis, Visualization, Writing - original draft, Software. **Wei Gong:** Resources, Writing - review & editing, Supervision, Data curation. **Shihua Chen:** Resources, Writing - review & editing, Supervision, Data curation. **Shikuan Jin:** Writing - review & editing, Software. **Jun Wang:** Writing - review & editing.

#### Acknowledgements

This work was supported by the National Key R&D Program of China (Grant No. 2018YFB0504500, and No.2017YFC0212600), the National Natural Science Foundation of China (Grant No. 41905032, No. 41875038, No. 41801261 and No. 41627804), the Natural Science Foundation of Hubei Province (Grant No. 2017CFB404), the Wuhan Science and Technology Plan (Grant NO. 2019020701011453), the Wuhan University Luojia Talented Young Scholar Project. We are grateful to Japan Aerospace Exploration Agency and National Institute of Environmental Studies (<http://www.eorc.jaxa.jp/ptree/index.html>) for providing excellent and accessible data products. We are also grateful to Institute of Remote Sensing and Digital Earth, Chinese Academy of Sciences for their improved dark target method aiming to AHI.

#### References

Ackerman, Strabala, Menzel, Frey, Moeller, Gumley, 1998. Discriminating clear sky from clouds with MODIS. *J. Geophys. Res.* 103 (D24), 32141–32157.  
Anderson, Wang, Zeng, Leptoukh, Petrenko, Ichoku, Hu, 2013. Long-term statistical assessment of Aqua-MODIS aerosol optical depth over coastal regions: bias

characteristics and uncertainty sources. *Tellus B* 65, 20805. <https://doi.org/10.3402/tellusb.v65i0.20805>.  
Ångström, 1929. On the atmospheric transmission of sun radiation and on dust in the air. *Geogr. Ann.* 11 (2), 156–166.  
Atwater, 1970. Planetary albedo changes due to aerosols. *Science* 170 (3953), 64–66.  
Bellouin, et al., 2005. Global estimate of aerosol direct radiative forcing from satellite measurements. *Nature* 438 (7071), 1138.  
Bessho, et al., 2016. An introduction to Himawari-8/9—Japan's new-generation geostationary meteorological satellites. *J. Meteorol. Soc. Jpn.* Ser. II 94 (2), 151–183.  
Carslaw, et al., 2013. Large contribution of natural aerosols to uncertainty in indirect forcing. *Nature* 503 (7474), 67.  
Charlson, et al., 1992. Climate forcing by anthropogenic aerosols. *Science* 255 (5043), 423–430.  
Che, et al., 2015. Fine mode aerosol optical properties related to cloud and fog processing over a cluster of cities in northeast China. *Aerosol Air Qual. Res.* 15 (5), 2065–2081. <https://doi.org/10.4209/aaqr.2014.12.0325>.  
Chooari, Zavar-Reza, Sturman, 2014. The global distribution of mineral dust and its impacts on the climate system: a review. *Atmos. Res.* 138, 152–165.  
Christopher, Wang, Ji, Tsay, 2003. Estimation of diurnal shortwave dust aerosol radiative forcing during PRIDE. *J. Geophys. Res.* 108, 8596. <https://doi.org/10.1029/2002JD002787>.  
Chu, et al., 2002. Validation of MODIS aerosol optical depth retrieval over land. *Geophys. Res. Lett.* 29 (12), MOD2-1.  
Dubovik, Smirnov, Holben, King, Kaufman, Eck, Slutsker, 2000. Accuracy assessment of aerosol optical properties retrieved from Aerosol Robotic Network (AERONET) Sun and sky radiance measurements. *J. Geophys. Res.* 105 (D8), 9791–9806.  
Eck, et al., 1999. Wavelength dependence of the optical depth of biomass burning, urban, and desert dust aerosols. *J. Geophys. Res.* 104 (D24), 31333–31349.  
Fukuda, Nakajima, Takenaka, Higurashi, Kikuchi, Nakajima, Ishida, 2013. New approaches to removing cloud shadows and evaluating the 380 nm surface reflectance for improved aerosol optical thickness retrievals from the GOSAT/TANSO-Cloud and Aerosol Imager. *J. Geophys. Res.* 118 (24), 13–520.  
Ge, Wang, Reid, 2014. Mesoscale modeling of smoke transport over the Southeast Asian Maritime Continent: coupling of smoke direct radiative feedbacks below and above the low-level clouds. *Atmos. Chem. Phys.* 14, 159–174.  
Ge, et al., 2016. Taklimakan Desert nocturnal low-level jet: climatology and dust activity. *Atmos. Chem. Phys.* 16 (12), 7773–7783.  
Ge, et al., 2019. A dark target method for himawari-8/AHI aerosol retrieval: application and validation. *IEEE Trans. Geosci. Rem. Sens.* 57 (1), 381–394. <https://doi.org/10.1109/grs.2018.28547.43>.  
Gupta, P., Levy, R.C., Mattoo, S., Remer, L.A., Holz, R.E., Heidinger, A.K., 2019. Applying the dark target aerosol algorithm with advanced Himawari imager observations during the KORUS-AQ field campaign. *Atmospheric Measurement Techniques* 12, 6557–6577.  
Hartmann, 2015. *Global Physical Climatology*, vol. 103. Newnes.  
Higurashi, Nakajima, 1999. Development of a two-channel aerosol retrieval algorithm on a global scale using NOAA AVHRR. *J. Atmos. Sci.* 56 (7), 924–941.  
Hinds, 1999. *Aerosol Technology: Properties, Behavior, and Measurement of Airborne Particles*. John Wiley & Sons.  
Holben, et al., 1998. AERONET—a federated instrument network and data archive for aerosol characterization. *Remote Sens. Environ.* 66 (1), 1–16.  
Holben, et al., 2001. An emerging ground-based aerosol climatology: aerosol optical depth from AERONET. *J. Geophys. Res.* 106 (D11), 12067–12097.  
Huang, et al., 2016. Validation and expected error estimation of Suomi-NPP VIIRS aerosol optical thickness and Ångström exponent with AERONET. *J. Geophys. Res.* 121 (12), 7139–7160.  
Huang, Wang, Wang, Li, Yan, 2014. Climate effects of dust aerosols over East Asian arid and semiarid regions. *J. Geophys. Res.* 119 (19), 11–398.  
Ishida, Nakajima, 2009. Development of an unbiased cloud detection algorithm for a spaceborne multispectral imager. *J. Geophys. Res.* 114 (D7).  
Ishida, Nakajima, Yokota, Kikuchi, Watanabe, 2011. Investigation of GOSAT TANSO-CAI cloud screening ability through an intersatellite comparison. *J. Appl. Meteorol. Clim.* 50 (7), 1571–1586.  
Jin, et al., 2019. Retrieval of 500 m aerosol optical depths from MODIS measurements over urban surfaces under heavy aerosol loading conditions in winter. *Rem. Sens.* 11.  
Kahnet, et al., 2005. Multiangle Imaging Spectroradiometer (MISR) global aerosol optical depth validation based on 2 years of coincident Aerosol Robotic Network (AERONET) observations. *J. Geophys. Res.* 110 (D10).  
Karimipour, Ghandehari, 2013. Voronoi-based medial axis approximation from samples: issues and solutions. *Transactions on Computational Science XX*, 138–157. Springer.  
Kaufman, Tanré, 1998. Algorithm for remote sensing of tropospheric aerosol from MODIS. NASA MODIS algorithm theoretical basis document. Goddard Space Flight Center 85, 3–68.  
Kaufman, Tanré, Remer, Vermote, Chu, Holben, 1997. Operational remote sensing of tropospheric aerosol over land from EOS moderate resolution imaging spectroradiometer. *J. Geophys. Res.* 102 (D14), 17051–17067.  
Kokhanovsky, 2009. In: Leeuw, G. (Ed.), *Satellite Aerosol Remote Sensing over Land*. Springer, Berlin.  
Lennartson, et al., 2018. Diurnal variation of aerosol optical depth and PM 2.5 in South Korea: a synthesis from AERONET, satellite (GOCl), KORUS-AQ observation, and the WRF-Chem model. *Atmos. Chem. Phys.* 18 (20), 15125–15144.  
Levy, 2009. The dark-land MODIS collection 5 aerosol retrieval: algorithm development and product evaluation. In: *Satellite Aerosol Remote Sensing over Land*. Springer, Berlin, Heidelberg, pp. 19–68.

- Levy, et al., 2010. Global evaluation of the Collection 5 MODIS dark-target aerosol products over land. *Atmos. Chem. Phys.* 10 (21), 10399–10420.
- Levy, et al., 2013. The Collection 6 MODIS aerosol products over land and ocean. *Atmos. Meas. Tech.* 6 (11), 2989–3034. <https://doi.org/10.5194/amt-6-2989-2013>.
- Levy, Remer, Dubovik, 2007a. Global aerosol optical properties and application to Moderate Resolution Imaging Spectroradiometer aerosol retrieval over land. *J. Geophys. Res.* 112 (D13) <https://doi.org/10.1029/2006jd007815> n/a-n/a.
- Levy, Remer, Mattoo, Vermote, Kaufman, 2007b. Second-generation operational algorithm: retrieval of aerosol properties over land from inversion of Moderate Resolution Imaging Spectroradiometer spectral reflectance. *J. Geophys. Res.* 112 (D13) <https://doi.org/10.1029/2006jd007811> n/a-n/a.
- Li, Remer, Kaufman, Mattoo, Gao, Vermote, 2005. Snow and ice mask for the MODIS aerosol products. *IEEE Geosci. Remote S.* 2 (3), 306–310.
- Li, et al., 2018. Long-term variation of cloud droplet number concentrations from space-based Lidar. *Remote Sens. Environ.* 213, 144–161.
- Liou, 2002. *An Introduction to Atmospheric Radiation*. Elsevier.
- Liu, Ma, Gong, Zhang, Wang, Shi, 2018a. Comparison of AOD from CALIPSO, MODIS, and sun photometer under different conditions over Central China. *Sci. Rep.* 8 (1), 10066 <https://doi.org/10.1038/s41598-018-28417-7>.
- Liu, Ma, Gong, Zhang, Yang, 2018b. Determination of boundary layer top on the basis of the characteristics of atmospheric particles. *Atmos. Environ.* 178, 140–147.
- Liu, et al., 2014a. Preliminary evaluation of S-NPP VIIRS aerosol optical thickness. *J. Geophys. Res.* 119 (7), 3942–3962.
- Liu, Shen, Gao, Liu, Sun, 2014b. Evaluation of CALIPSO aerosol optical depth using AERONET and MODIS data over China. In: *Remote Sensing and Modeling of Ecosystems for Sustainability XI*, vol. 9221, p. 92210F.
- Martins, Tanré, Remer, Kaufman, Mattoo, Levy, 2002. MODIS cloud screening for remote sensing of aerosols over oceans using spatial variability. *Geophys. Res. Lett.* 29 (12), MOD4-1.
- McCormick, Ludwig, 1967. Climate modification by atmospheric aerosols. *Science* 156 (3780), 1358–1359.
- Mitchell, 1971. The effect of atmospheric aerosols on climate with special reference to temperature near the earth's surface. *J. Appl. Meteorol.* 10 (4), 703–714.
- Nakajima, Tanaka, Yamano, Shiobara, Arai, Nakanishi, 1989. Aerosol optical characteristics in the yellow sand events observed in May, 1982 at Nagasaki-Part II Models. *J. Meteorol. Soc. Jpn.* Ser. II 67 (2), 279–291.
- Nakajima, Tanaka, 1988. Algorithms for radiative intensity calculations in moderately thick atmospheres using a truncation approximation. *J. Quant. Spectrosc. Ra.* 40 (1), 51–69.
- Nichol, Bilal, 2016. Validation of MODIS 3 km resolution aerosol optical depth retrievals over Asia. *Rem. Sens.* 8 (4), 328.
- Omar, Won, Winker, Yoon, Dubovik, McCormick, 2005. Development of global aerosol models using cluster analysis of Aerosol Robotic Network (AERONET) measurements. *J. Geophys. Res.* 110 (D10).
- Pollack, Cuzzi, 1980. Scattering by nonspherical particles of size comparable to a wavelength: a new semi-empirical theory and its application to tropospheric aerosols. *J. Atmos. Sci.* 37 (4), 868–881.
- Remer, Kaufman, 1998. Dynamic aerosol model: urban/industrial aerosol. *J. Geophys. Res.*: Atmosphere 103, 13859–13871.
- Remer, et al., 2002. Validation of MODIS aerosol retrieval over ocean. *Geophys. Res. Lett.* 29 (12), MOD3-1.
- Remer, et al., 2005. The MODIS aerosol algorithm, products, and validation. *J. Atmos. Sci.* 62 (4), 947–973.
- Rodgers, 2000. *Inverse Methods for Atmospheric Sounding: Theory and Practice*, vol. 2. World scientific.
- Stamnes, Tsay, Wiscombe, Jayaweera, 1988. Numerically stable algorithm for discrete-ordinate-method radiative transfer in multiple scattering and emitting layered media. *Appl. optics* 27 (12), 2502–2509.
- Tao, et al., 2015. Comparison and evaluation of the MODIS Collection 6 aerosol data in China. *J. Geophys. Res.* 120, 6992–7005.
- Tao, et al., 2017a. Evaluation of MODIS Deep Blue aerosol algorithm in desert region of East Asia: ground validation and intercomparison. *J. Geophys. Res.* 122, 10357–10368.
- Tao, et al., 2017b. How do aerosol properties affect the temporal variation of MODIS AOD bias in eastern China? *Rem. Sens.* 9 (8), 800.
- Tegen, Lacis, 1996. Modeling of particle size distribution and its influence on the radiative properties of mineral dust aerosol. *J. Geophys. Res.* 101 (D14), 19237–19244.
- Wang, et al., 2003a. Geostationary satellite retrievals of aerosol optical thickness during ACE-Asia. *J. Geophys. Res.* 108, 8657. <https://doi.org/10.1029/2003JD003580>.
- Wang, et al., 2003b. GOES-8 retrieval of dust aerosol optical thickness over the Atlantic Ocean during PRIDE. *J. Geophys. Res.* 108, 8595. <https://doi.org/10.1029/2002JD002494>.
- Wang, Liu, Christopher, Reid, Maring, 2003c. The effects of non-sphericity on geostationary satellite retrievals of dust aerosols. *Geophys. Res. Lett.* 30, 2293. <https://doi.org/10.1029/2003GL018697>.
- Wang, Martin, 2007. Satellite characterization of urban aerosols: Importance of including hygroscopicity and mixing state in the retrieval algorithms. *J. Geophys. Res.* 112 (D17).
- Wang, Xu, Henze, Zeng, Ji, Tsay, Huang, 2012. Top-down estimate of dust emissions through integration of MODIS and MISR aerosol retrievals with the GEOS-Chem adjoint model. *Geophys. Res. Lett.* L08802 <https://doi.org/10.1029/2012GL051136>.
- Wang, Xu, Spurr, Wang, Drury, 2010. Improved algorithm for MODIS satellite retrievals of aerosol optical thickness over land in dusty atmosphere: Implications for air quality monitoring in China. *Remote Sens. Environ.* 114, 2575–2583.
- Wang, Christopher, 2003. Intercomparison between satellite-derived aerosol optical thickness and PM2.5 mass: implications for air quality studies. *Geophys. Res. Lett.* 30 (21).
- Wang, Gong, Xia, Zhu, Li, Zhu, 2015. Long-term observations of aerosol optical properties at Wuhan, an urban site in Central China. *Atmos. Environ.* 101, 94–102. <https://doi.org/10.1016/j.atmosenv.2014.11.021>.
- Wang, Mao, Du, Pan, Gong, 2017a. Validation of VIIRS AOD through a comparison with a sun photometer and MODIS AODs over wuhan. *Rem. Sens.* 9 (5), 403.
- Wang, Mao, Du, Pan, Gong, Fang, 2017b. Deriving hourly PM2.5 concentrations from himawari-8 AODs over beijing-tianjin-hebei in China. *Rem. Sens.* 9 (8) <https://doi.org/10.3390/rs9080858>.
- Wang, et al., 2019. Two-stage model for estimating the spatiotemporal distribution of hourly PM1.0 concentrations over central and east China. *Sci. Total Environ.* 675, 658–666.
- Wei, et al., 2019. MODIS Collection 6.1 aerosol optical depth products over land and ocean: validation and comparison. *Atmos. Environ.* 201, 428–440.
- WHO, 2000. Air quality guidelines for europe. *J. Toxicol. Environ. Health Part A* 71 (91).
- Winker, et al., 2009. Overview of the CALIPSO mission and CALIOP data processing algorithms. *J. Atmos. Ocean. Technol.* 26 (11), 2310–2323.
- Winker, et al., 2010. The CALIPSO mission: a global 3D view of aerosols and clouds. *Bull. Am. Meteorol. Soc.* 91 (9), 1211–1230.
- Wu, Zhu, Che, Xia, Zhang, 2015. Column-integrated aerosol optical properties and direct radiative forcing based on sun photometer measurements at a semi-arid rural site in Northeast China. *Atmos. Res.* 157, 56–65.
- Xiao, et al., 2016. Evaluation of VIIRS, GOCI, and MODIS Collection 6 AOD retrievals against ground sunphotometer observations over East Asia. *Atmos. Chem. Phys.* 16 (3), 1255–1269.
- Xu, et al., 2002. Measurement of aerosol chemical, physical and radiative properties in the Yangtze delta region of China. *Atmos. Environ.* 36 (2), 161–173.
- Xu, Wang, 2015. Retrieval of aerosol microphysical properties from aeronet photopolarimetric measurements: 1. information content analysis. *J. Geophys. Res.* 120 (14), 7059–7078.
- Yoshida, Kikuchi, Nagao, Murakami, Nomaki, Higurashi, 2018. Common retrieval of aerosol properties for imaging satellite sensors. *J. Meteorol. Soc. Jpn.* Ser. II.
- Yu, et al., 2006. A review of measurement-based assessments of the aerosol direct radiative effect and forcing. *Atmos. Chem. Phys.* 6 (3), 613–666.
- Zhang, et al., 2017a. Aerosol radiative effect in UV, VIS, NIR, and SW spectra under haze and high-humidity urban conditions. *Atmos. Environ.* 166, 9–21.
- Zhang, et al., 2017b. Aerosol optical properties and direct radiative effects over Central China. *Rem. Sens.*
- Zhang, Ma, Gong, Liu, Shi, Chen, 2018. Aerosol optical properties and radiative effects: assessment of urban aerosols in central China using 10-year observations. *Atmos. Environ.* 182, 275–285. <https://doi.org/10.1016/j.atmosenv.2018.03.040>.
- Zhang, et al., 2019. Validation of Himawari-8 aerosol optical depth retrievals over China. *Atmos. Environ.* 199, 32–44. <https://doi.org/10.1016/j.atmosenv.2018.11.024>.